

Supporting Information

Impact of iodine loading and substitution position on intersystem crossing efficiency in a series of ten methylated-*mesophenyl*-BODIPY dyes

Jack T. Ly^{a,b}, Kayla F. Presley^a, Thomas M. Cooper^a, Luke A. Baldwin^a, Matthew J. Dalton^a, and Tod A. Grusenmeyer^a

^a*Air Force Research Laboratory, Materials and Manufacturing Directorate, Wright-Patterson Air Force Base, Dayton, Ohio 45433, United States*

^b*UES, Inc., Dayton, Ohio 45432, United States*

Table of Contents

Materials and Methods	S3
Synthesis, ^1H and ^{13}C NMR, FTIR and Mass Spectrometry	S7
Supplementary Figures and Table	S24
DFT Results	S34
References	S43

Materials and Methods

General considerations. Inert atmospheric syntheses were carried out using standard Schlenk line techniques. Mass spectrometry data was collected at the Campus Chemical Instrument Center (CCIC) at the Ohio State University using a 15T Bruker SolarixR Fourier transform ion cyclotron resonance (FT-ICR) instrument. Laser desorption ionization (LDI) method was used in the positive ion mode. For LDI, the samples were deposited on a standard, stainless steel MALDI plate without using any matrix. A Nd:YAG laser was used at 351 nm for ionization/desorption. The laser power was varied in the range of 20-25%. The resolution of the mass spectrometer was set to about 300,000 (at m/z 400), and the mass measurement accuracy was < 2ppm in all cases. For calibration, a Bruker peptide mixture was used for LDI. Chemical reagents and solvents were purchased from a combination of Sigma Aldrich, TCI America, and Acros Organics and were used as-received. ^1H NMR experiments were performed on a Bruker Avance III HD 400 NMR spectrometer operating at 400 MHz. ^{13}C NMR was performed on an OXFORD AS600 NMR spectrometer operating at 600 MHz. NMR experiments were run at millimolar concentrations. Absolute fluorescence quantum yield, relative $^1\text{O}_2$ phosphorescence quantum yield, and lifetime emission measurements were collected in duplicate. All supplementary figures presented are representative of the first trial of data collection.

Instrumentation. Ground-state UV/vis absorption spectra measurements and extinction coefficients were determined using a Cary 5000 and a Cary 500 spectrophotometer. Steady-state fluorescence and 77 K phosphorescence spectra were obtained using an Edinburgh Instruments FLS1000 spectrometer. Samples were excited using a 450 W xenon lamp attached to a Czerny-Turner double monochromator (focal length: 2 x 325 mm) or a pulsed xenon microsecond flashlamp operated at 40 Hz. The emission signal was collected at 90° relative to the excitation source and passed through a single grating Czerny-Turner monochromator (focal length: 325 mm). An extended red photomultiplier tube (PMT) detector with spectral range from 200 – 980 nm is in a cooled housing and was run at an operating temperature of -22 °C. Luminescence lifetimes and photosensitized singlet oxygen phosphorescence spectra were collected using an Edinburgh Instruments FLS980 spectrometer. Samples were excited using a 450 W xenon lamp attached to a Czerny-Turner monochromator (300 nm focal length, 1800 grooves/mm grating, 1.8 nm/mm linear dispersion) or a pulsed diode laser. The emission signal was collected at 90° relative to the excitation source and passed through a Czerny-Turner monochromator (300 nm focal length, 1800 grooves/mm grating, 1.8 nm/mm linear dispersion) prior to being collected with a Hamamatsu R928P side window photomultiplier in a cooled housing (Operating temperature: -20 °C) for visible luminescence or a Hamamatsu R5509-72 photomultiplier in a nitrogen-flow cooled housing (Operating temperature: -80 °C) for NIR luminescence. ATR-FTIR spectra were collected using a Bruker-Alpha P ATR-FTIR with OPUS software.

Ground-state absorption, excitation spectra, and steady-state luminescence. Extinction coefficient determinations were performed via four serial dilutions of 1.0 – 1.3 mg of dye in 100 mL of toluene stock solution. Excitation scans were also conducted with emission set at the low energy shoulder or maximum of the 0-1 transition in the fluorescence spectrum. Excitation scans were measured with the emission bandwidth at 3 nm and the excitation bandwidth at 1 nm with the excitation source ranging between 300-800 nm. Superposition of the excitation spectra with the ground state absorption spectra provides confidence that the observed luminescence results from the designated BODIPY derivative and not an impurity. (**Figure S23-S25**). Steady-state fluorescence spectra was carried out with excitation and emission bandwidths at 1 nm. Spectral range of steady-state fluorescence spectra varied accordingly: 490-900 nm

for **BDP/I-BDP**, 510-900 nm for **I₂-BDP/I₃-BDP**, 600-900 nm for **BDP-0/I-BDP-0**, and 610-900 nm for **BDP-2, I-BDP-2, I₂-BDP-0**, and **I₂-BDP-2**. Steady-state phosphorescence spectra of the four core BDP derivatives, **BDP, I-BDP, I₂-BDP**, and **I₃-BDP**, were collected in 2:2:1:1 (v:v) ethyl iodide, diethyl ether, ethanol, toluene glass at 77 K. The use of iodine containing solvents in low temperature glasses is known to facilitate phosphorescence via an external heavy atom effect.^{1,2} The phosphorescence spectra of the 2,6-diiodo substituted derivatives, **I₂-BDP** and **I₃-BDP**, were carried out with an excitation bandwidth of 1 nm and an emission bandwidth of 0.5 nm. The luminescence signal was collected from 520-900 nm. The phosphorescence spectra of the non-2,6-diiodo substituted derivatives, **BDP** and **I-BDP**, were collected with a gate delay on the luminescence detector. Gate Delay was used to avoid tailing fluorescence that overlaps the phosphorescence signal. The gated phosphorescence spectra were collected with a lamp frequency of 40 Hz, a gate delay of 1 ms, and a gate width of 8 ms. The spectra were collected with an excitation bandwidth of 5 nm and an emission bandwidth of 1 nm. The luminescence signal was collected from 490-900 nm.

Fluorescence Lifetimes. Fluorescence lifetime fitting was performed using the Fluoracle software package (Edinburgh Instruments). All of the fluorescence lifetime data were fit using monoexponential decay fits. A reconvolution fit was utilized to take into account the presence of the instrument response function (IRF). The reconvolution fit range was started at the mid-rise of the luminescence signal and included the data points until approximately 4 e-folds worth of luminescence decay had occurred. All samples were excited using a 404 nm pulsed diode laser source with a pulse width of 58.8 ps. The luminescence was collected at the maximum of the respective fluorescence spectrum. The slit widths of fluorescence lifetime measurements varied as the emission counts were set to be 2-4% of the excitation counts of the source. Variation of slit widths were due to differences in quantum yields of the chromophores. Representative data and fits for a single trial of the core BDP, non-triplet forming distyryl-BDP, and triplet forming distyryl-BDP derivatives are provided in **Figures S26, S27, and S28**, respectively.

Absolute Fluorescence Quantum Yield Measurements. Fluorescence quantum yields, ϕ_F , were determined using an integrating sphere in conjunction with the Edinburgh Instruments FLS980 spectrometer. Detailed discussion of collecting and calculating absolute quantum yields using an integrating sphere is previously described.³ The excitation intensity was set with a blank toluene solution in the sample chamber. Emission slits and excitation slits were chosen to achieve ~1 million counts at the excitation wavelength as observed on the PMT. Experimental setup parameters (emission slit width, excitation slit width, and emission range) were varied for the four different excitation wavelengths:

- I. 480 nm excitation wavelength, 0.153 nm emission slit, 3.4 nm excitation slit, and 470 to 750 nm emission range experimental parameters were set for **BDP** and **I-BDP**.
- II. 510 nm excitation wavelength, 0.162 nm emission slit, 3.879 nm excitation slit, and 500 to 800 nm emission range experimental parameters were set for **I₂-BDP** and **I₃-BDP**.
- III. 577 nm excitation wavelength, 0.243 nm emission slit, 4.5 nm excitation slit, and 565 to 850 nm emission range experimental parameters were set for **I-BDP-0** and **BDP-0**.
- IV. 600 nm excitation wavelength, 0.28 nm emission slit, 5 nm excitation slit, and 590 to 850 nm emission range experimental parameter were set for **BDP-2, I₂-BDP-2, I-BDP-2**, and **I₂-BDP-0**.

Each fluorescence spectra was averaged over three scans and was collected using a 0.5 nm step size and a dwell time of 0.5 s. The total photons absorbed by a particular BDP sample were obtained by subtracting the integrated excitation intensity for the BDP sample from the integrated excitation intensity of the

toluene blank. The raw fluorescence intensity signal was integrated from the crossing point of the toluene blank signal and the BDP sample signal on the red-end of the fluorescence spectrum. This integration procedure was completed using the Edinburgh Instruments Fluoracle software package. A ground-state reabsorption correction was applied to all of the fluorescence spectra. The concentrated samples had a ground state absorption value between 0.1-0.2 at the excitation wavelength. The dilute samples used in the correction were a 10x serial dilution of the concentrated sample used for each data trial. The data used to determine the fluorescence quantum yield values for all of the dyes are shown in **Figure S29-S31**.

Relative Luminescence Quantum Yield Measurements. The photosensitized singlet oxygen phosphorescence quantum yields were determined using relative quantum yield measurements. These measurements are used to approximate the intersystem crossing quantum yield for each sample. The photosensitized singlet oxygen quantum yield is taken as the lower limit of the intersystem crossing yield, because diffusional deactivation of the chromophore excited state by ground state oxygen does not have to produce phosphorescent singlet oxygen.⁴ A discussion of relevant luminescence quantum yield standards and a detailed overview of the collection of relative quantum yield measurements are summarized elsewhere.^{5,6} The equation used to determine the luminescence quantum yield of a sample using a reference standard is given in equation S1,

$$(S1) \quad \Phi_x = \frac{F_x f_x(\lambda_{ex,x}) \eta_x^2}{F_{std} f_{std}(\lambda_{ex,std}) \eta_{std}^2} \Phi_{f,std}$$

where $\Phi_{f,std}$ is the reference standard emission quantum yield, F_x and F_{std} are the integrated luminescence intensity values obtained from the unknown and reference standard, $f_x(\lambda_{ex,x})$ and $f_{std}(\lambda_{ex,std})$ are the fraction of light absorbed by the unknown and reference standard, and η_x^2 and η_{std}^2 are index of refraction for the unknown and reference standard solvent. The index of fraction correction is only applied when solvents between the unknown and standard differ. Given all measurements are conducted in the same solution, the refractive index terms were omitted when calculating the relative quantum yield values. The photosensitized singlet oxygen phosphorescence quantum yields for the BDP dyes were determined using phenazine as a reference standard. All samples were absorbance matched and excited at 361 nm. Experimental parameters for each measurement were as follows: excitation slits at 3 nm, emission slits at 21 nm, averaged over 50 scans, and luminescence signal collected from 1240-1330 nm. The singlet oxygen emission spectra were integrated from 1250 - 1320 nm. A photosensitized singlet oxygen quantum yield value of 0.88 was used for the phenazine reference sample.⁴ Luminescence data used to determine the singlet oxygen phosphorescence quantum yields are shown in **Figure S32-S34**.

Rate Constant Determination. Following the determination of the fluorescence lifetime (τ_s), fluorescence quantum yield (Φ_F), and the intersystem crossing quantum yield (Φ_T), all relevant rate constants can be determined by solving the series of equations S2 – S4.

$$(S2) \quad \tau_F = \frac{1}{k_r + k_{nr} + k_{ISC}}$$

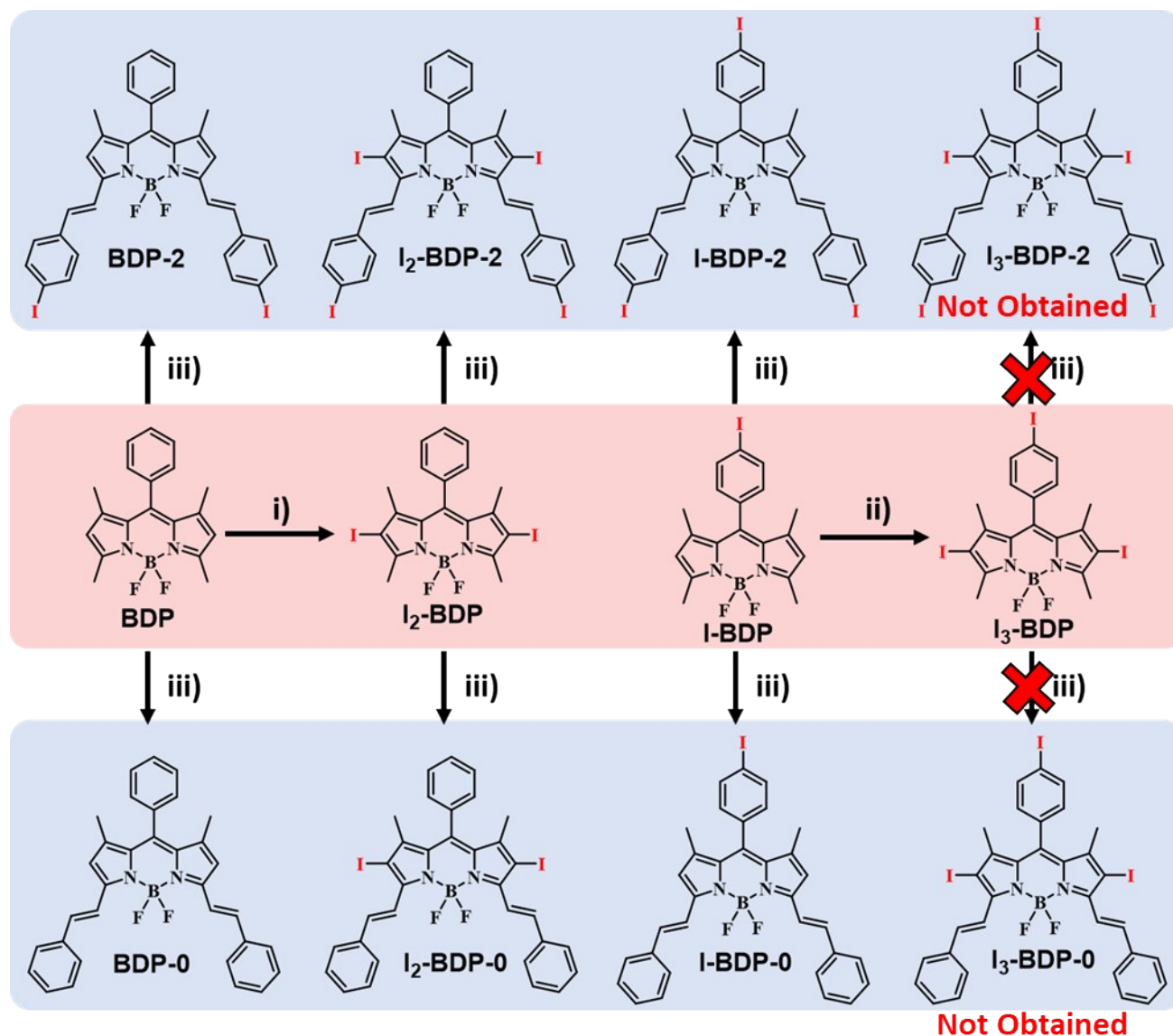
$$(S3) \quad \Phi_F = \frac{k_r}{k_r + k_{nr} + k_{ISC}}$$

$$(S4) \quad \Phi_T = \frac{k_{ISC}}{k_r + k_{nr} + k_{ISC}}$$

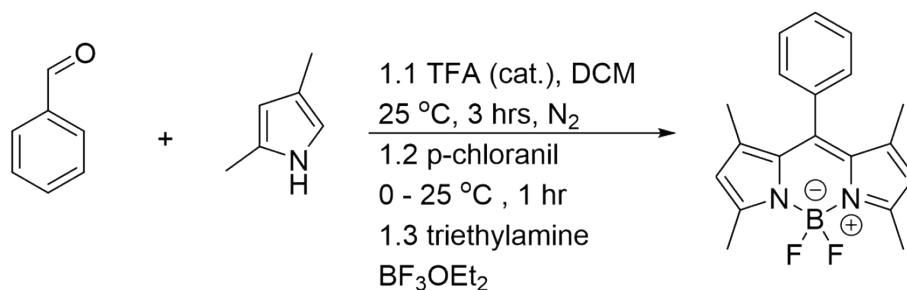
Photostability Testing. Photostability tests were conducted using the following mounted LEDs: a 505 nm cyan LED (M505L4, ThorLabs) for **BDP**, a 530 nm green LED (M530L4, ThorLabs) for **I₂-BDP**, and red 617 nm LEDs (M617L4, ThorLabs) for **I₂-BDP-0** and **BDP-0**. LED light was collimated through the use of an adjustable collimation adapter (SM1U25-A, ThorLabs) and was then passed through two adjustable iris diaphragm apertures (ID36/M and ID25/M, ThorLabs) to achieve a spot size with a diameter of 8 mm on the front face of the cuvette. The cuvette was held in place using a shielded cuvette holder (Model: 13950, Newport Corporation). For each test, the LED power was adjusted using a T-Cube™ LED Driver (LEDD1B, ThorLabs) until a power of 2 mW was achieved on a photodiode power sensor (S120VC, ThorLabs) and a power meter console (PM100A, ThorLabs). The resultant irradiance on each sample was 3.98 mW/cm². Solutions of BODIPY dyes were prepared in toluene with peak LED irradiance wavelengths at 0.5-0.6 absorbance. Measurements were taken at 1 hour intervals, up to 6 hours. Pictures of the photoirradiation setup are shown in **Figure S35**, while **Figure S36** depicts the absorption spectra as a function of irradiation time.

DFT Calculations. Calculations were performed using Gaussian 16, Revision B.01.⁷ Ground-state, S₁ state and T₁ state energy minimizations (B3LYP/6-31g(d) for H, B, C, N, F and SDD for I) were performed assuming vacuum with frequency calculations shown to have no imaginary frequencies. Higher accuracy energy and dipole moments (B3LYP/6-311g(2d,p) for H, B, C, N, F and SDD for I) were calculated for the optimized ground state, S₁ state and T₁ state geometries assuming vacuum. TDDFT calculations (CAM-B3LYP/6-311g(2d,p) for H, B, C, N, F and SDD for I) included the polarizable continuum model to simulate a toluene solution.

Synthesis, NMR, and Mass Spectrometry



Scheme S1. Synthesis of core and distyryl-BDPs i) NIS, CH₂Cl₂, 12 hrs, RT. ii) I₂, HIO₃, EtOH, 3 hrs, 75 °C, iii) Ar-C=O, AcOH, Piperidine, NIS DMF/THF. Dye labeling follows an I_n-BDP-m nomenclature convention where the “n” subscript indicates the number of iodines positioned on the methylated-*mesophenyl*-BDP portion of the molecule and the “m” numeral refers to the number of iodine atoms present on the styryl extensions. I₃-BDP-2 and I₃-BDP-0 were not obtained and confidently purified to characterize photophysically due to poor solubility of these derivatives.



1,3,5,7-Tetramethyl-8-phenyl-4,4-difluoroboradiazaindacene (BDP)

An 80 mL anhydrous dichloromethane solution of benzaldehyde (2.42 g, 23 mmol) and 2,4-dimethylpyrrole (5 g, 53 mmol) was prepared in a 250 mL round bottom flask. Four drops of trifluoroacetic acid added and allow to stir at room temperature for 3 hours under nitrogen. Solution turned yellow. P-chloranil (5.62 g, 23 mmol) added to the solution at 0 °C and stirred for an additional hour at room temperature. Reaction turned dark red. Excess triethylamine (13.18 g, 18 mL, 130 mmol) added followed by dropwise addition of excess BF₃OEt₂ (25.94 g, 23 mL, 180 mmol) via syringe. Reaction stirred for an additional hour. Solution was vacuum filtered. Filtered solid was washed with dichloromethane. Organic solution collected was dried and purified via silica chromatography with hexanes/ethyl acetate 9:1 mixture. Product collected and dried yielding orange crystals. 2.62g (34%) yield. ¹H NMR (400 MHz, CDCl₃): 7.49-7.47 (m, 3H), 7.29-7.26 (m, 2H), 5.98 (s, 2H), 2.56 (s, 6H), 1.37 (s, 6H). MW: 324.18 g/mol. LDI-MS: **BDP** calculated mass: 325.16855. Found mass: 325.16810 (1.4 ppm error).

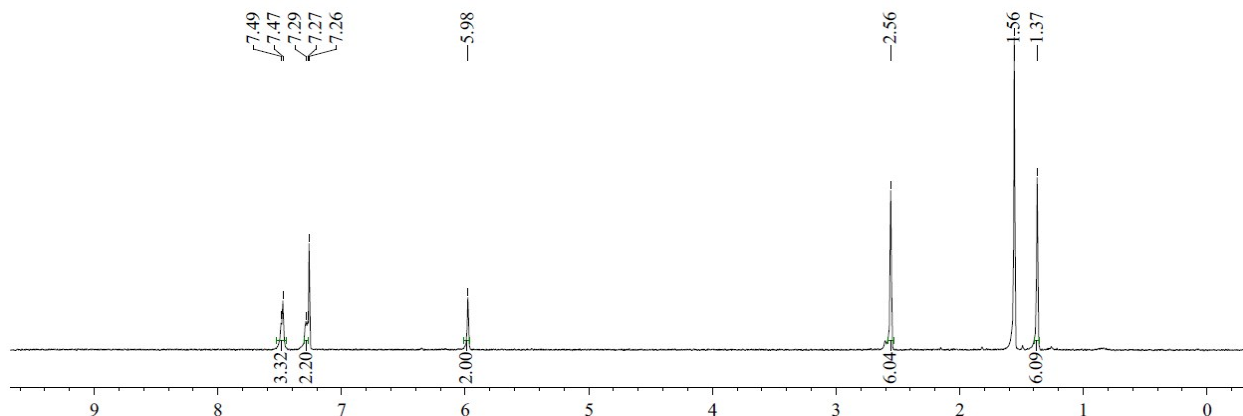


Figure S1. ¹H NMR of **BDP**.

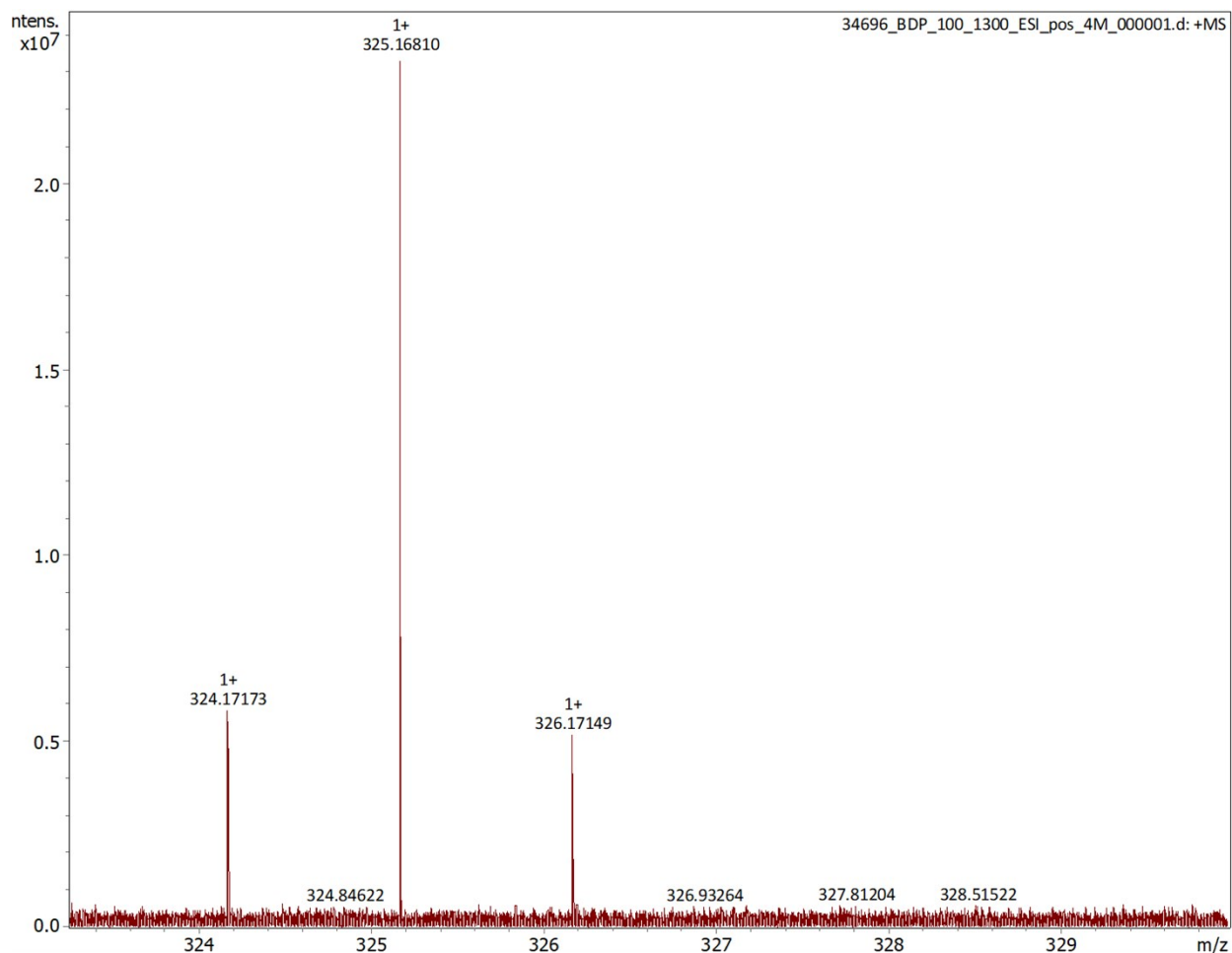
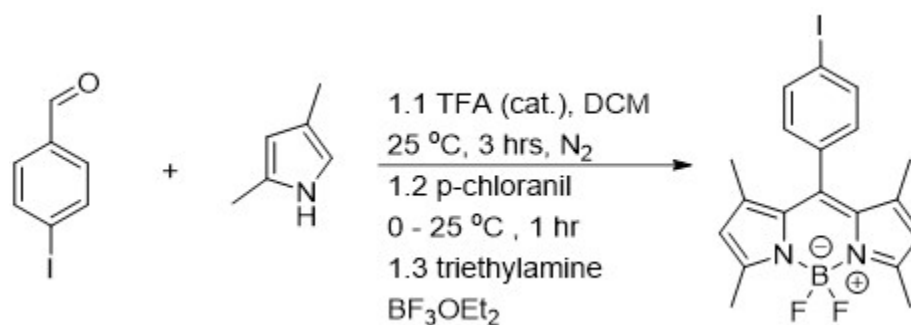


Figure S2. LDI-MS of BDP.



1,3,5,7-Tetramethyl-8-(*p*-iodophenyl)-4,4-difluoroboradiazaindacene (I-BDP**)**

A 40 mL anhydrous dichloromethane solution of 4-iodobenzaldehyde (2.65 g, 11.4 mmol) and 2,4-dimethylpyrrole (2.5 g, 26.2 mmol) was prepared in a 100 mL round bottom flask. Four drops of trifluoroacetic acid added and allow to stir at room temperature for 3 hours under nitrogen. Solution turned yellow. P-chloranil (2.8 g, 11.4 mmol) was added to the solution at 0 °C and stirred for an additional hour at room temperature. Reaction turned dark red. Excess triethylamine (6.58 g, 9.06 mL, 65 mmol)

added followed by dropwise addition of excess BF_3OEt_2 (12.95 g, 11.26 mL, 91.2 mmol) via syringe. Reaction stirred for an additional hour. Solution was vacuum filtered. Filtered solid was washed with dichloromethane. Organic solution collected was dried and purified via silica chromatography with hexanes/ethyl acetate 9:1 mixture. Product collected and dried yielding red/orange powder. 1.6 g (34%) yield. ^1H NMR (400 MHz, CDCl_3): 7.85 (d, 2H), 7.05 (d, 2H), 5.99 (s, 2H), 2.55 (s, 6H), 1.42 (s, 6H). MW: 450.8 g/mol. LDI-MS: **I-BDP** calculated mass: 450.05738. Found mass: 450.05768 (0.7 ppm error).

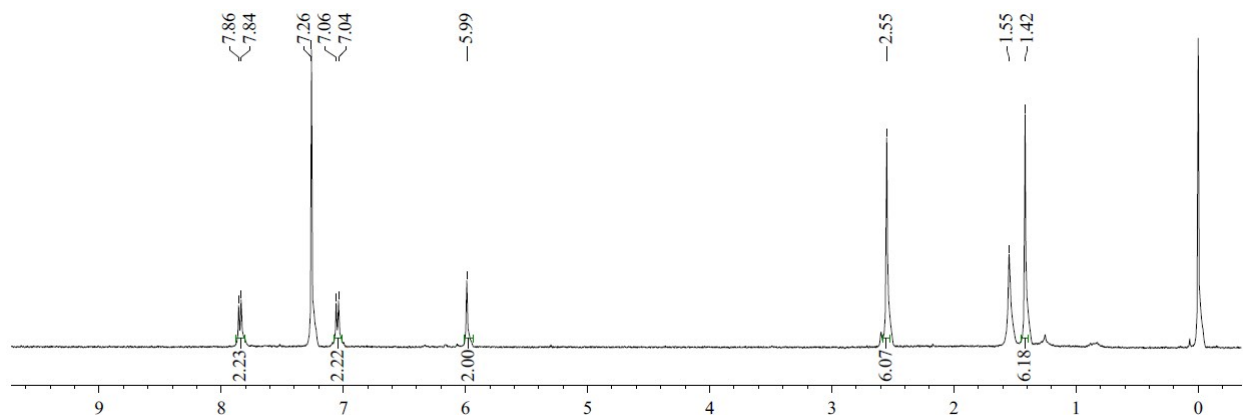


Figure S3. ^1H NMR of **I-BDP**.

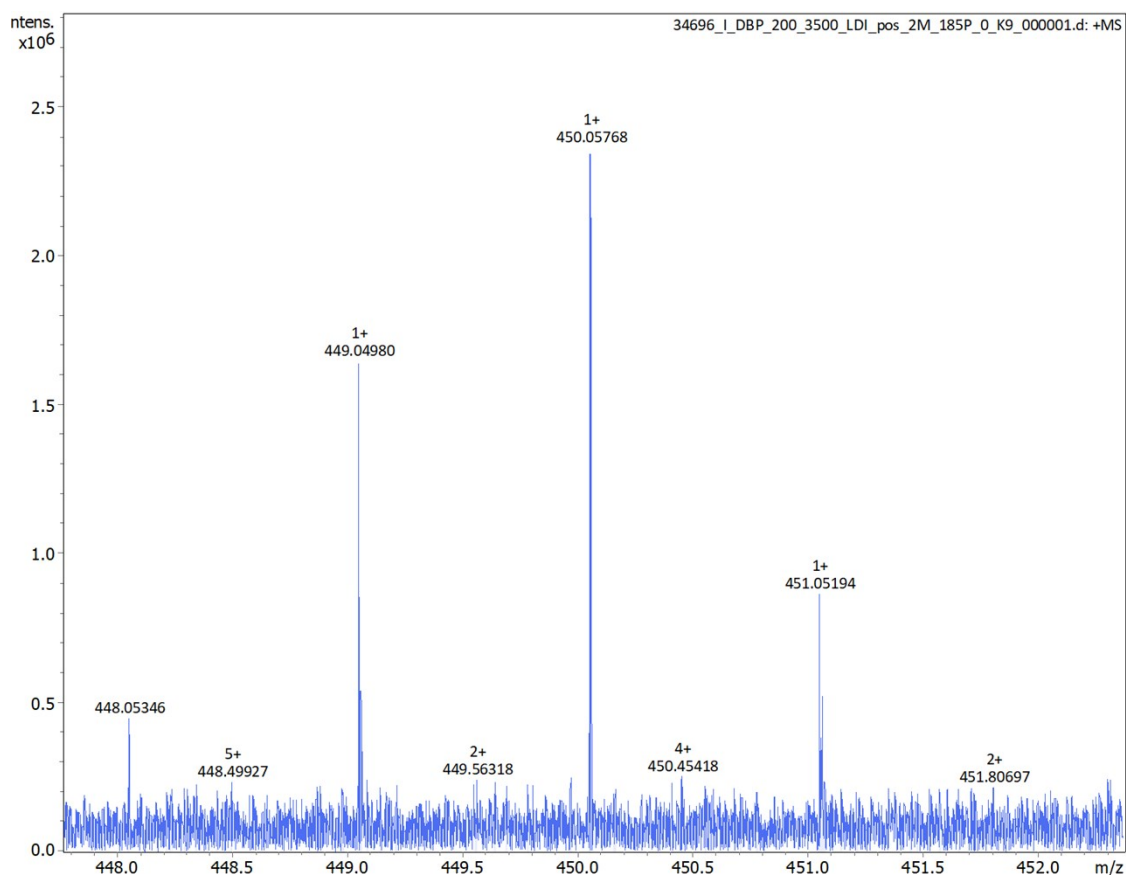
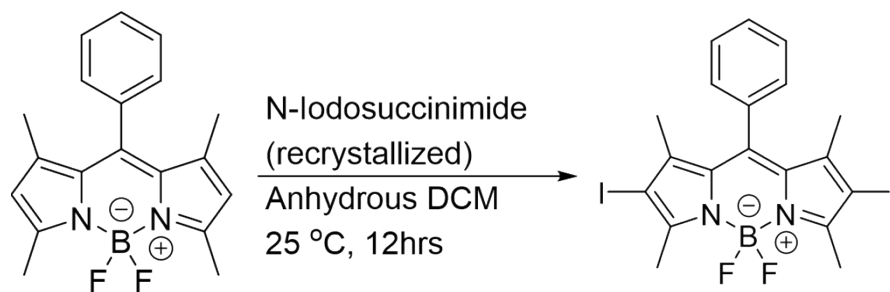


Figure S4. LDI-ToF of **I-BDP**.



2,6-Diiodo-1,3,5,7-tetramethyl-8-phenyl-4,4-difluoroboradiazasindacene (**I₂-BDP**)

BDP (2 g, 6.17 mmol) dissolved in 250 mL of anhydrous DCM. Recrystallized N-iodosuccinimide (5.55 g, 24.7 mmol) was added and stirred in the dark at room temperature for 12 hours. Organic solution washed with 10% sodium thiosulfate aqueous solution, organic solution collected, dried over sodium sulfate, and vacuum dried. Crude product purified via silica chromatography with hexanes/ethyl acetate 9:1 mixture. Product collected and dried yielding orange-like, green iridescent crystals. 3.2 g (87%) yield. ¹H NMR (400 MHz, CDCl₃): 7.53 (s, 3H), 7.26 (m, 2H), 2.65 (s, 6H), 1.38 (s, 6H). MW: 575.98 g/mol. LDI-MS: **I₂-BDP** calculated mass: 574.94620. Found mass: 574.94610 (0.2 ppm error).

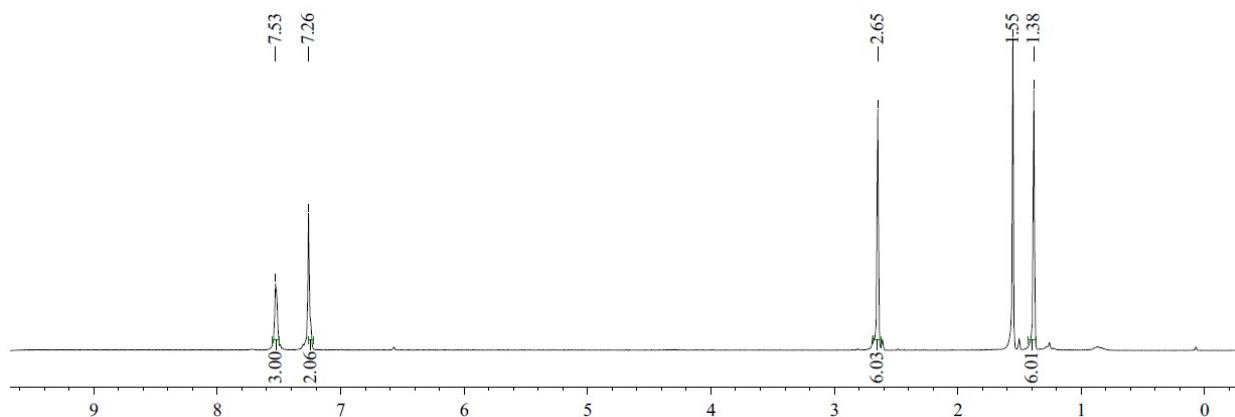


Figure S5. ¹H NMR of **I₂-BDP**.

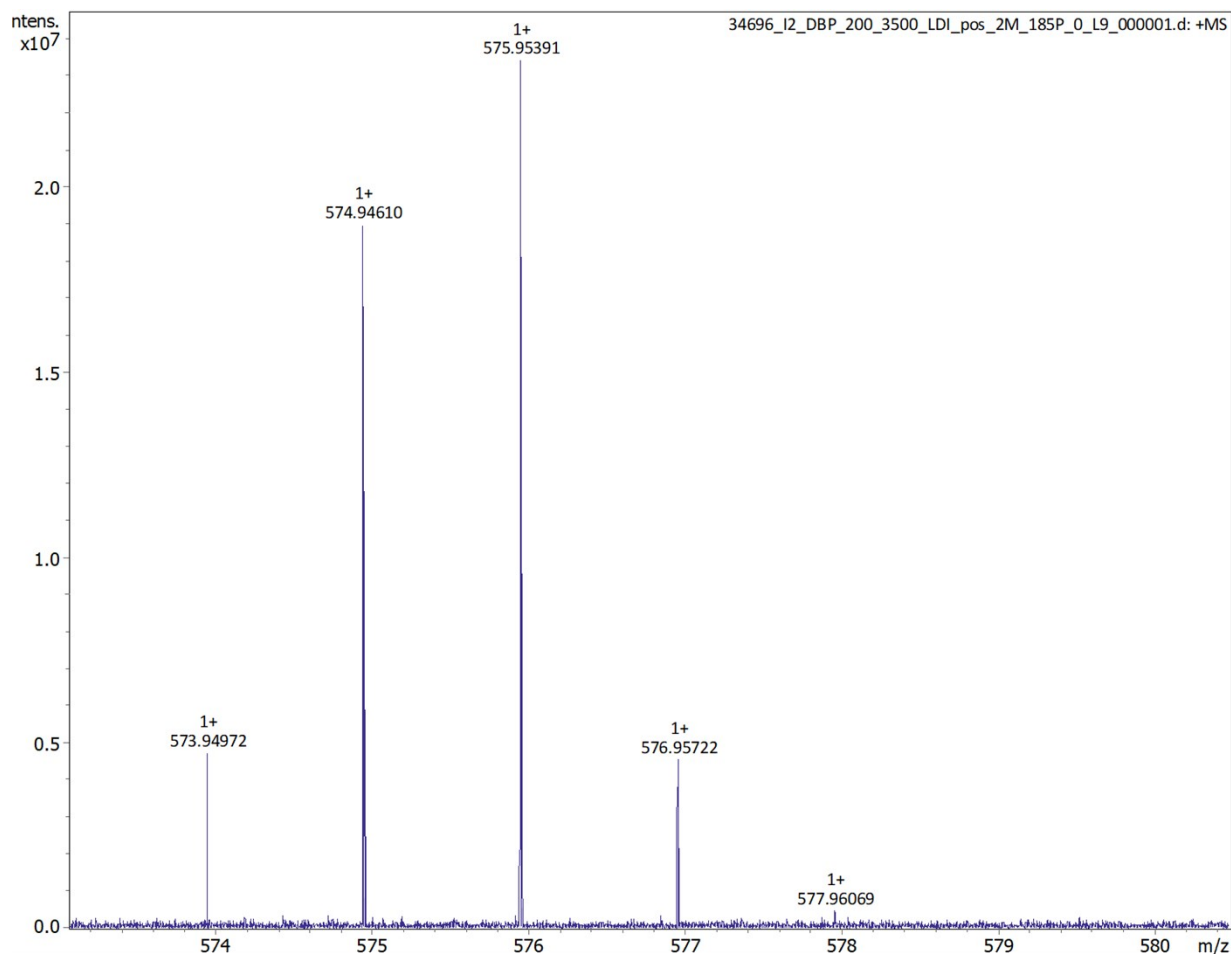
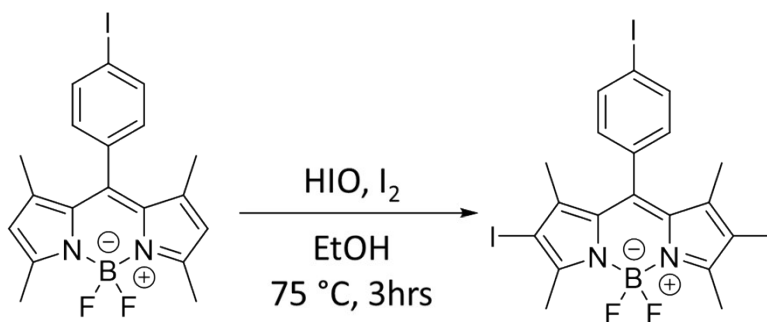


Figure S6. LDI-ToF of **I₂-BDP**.



2,6-Diiodo-1,3,5,7-Tetramethyl-8-(*p*-iodophenyl)-4,4-difluoroboradiazaindacene (**I₃-BDP**)

I-BDP (0.5 g, 1.11 mmol), iodic acid (0.284 g, 2.22 mmol), and iodine (0.703 g, 2.77 mmol) was dissolved in 50 mL of ethanol. Solution was heated to 75 °C for 3 hours. Reaction was cooled to room temperature,

filtered, and filtrate was rinsed with methanol to yield orange/red powder. 430 mg (55%) yield. ^1H NMR: 7.88 (d, 2H), 7.02 (d, 2H), 2.64 (s, 6H), 1.43 (s, 6H). MW: 701.87 g/mol. LDI-MS: $\text{I}_3\text{-BDP}$ calculated mass: 700.84285. Found mass: 700.84228 (0.8 ppm error).

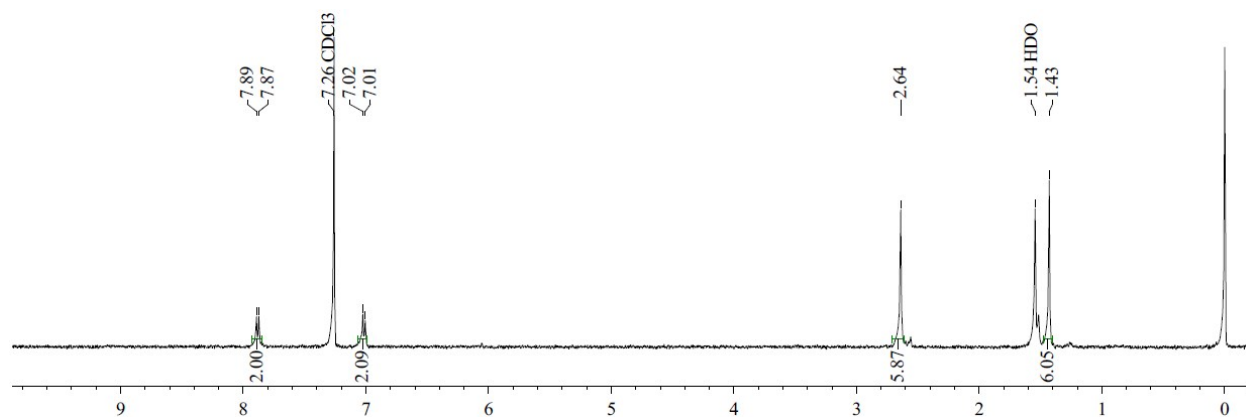


Figure S7. ^1H NMR of $\text{I}_3\text{-BDP}$.

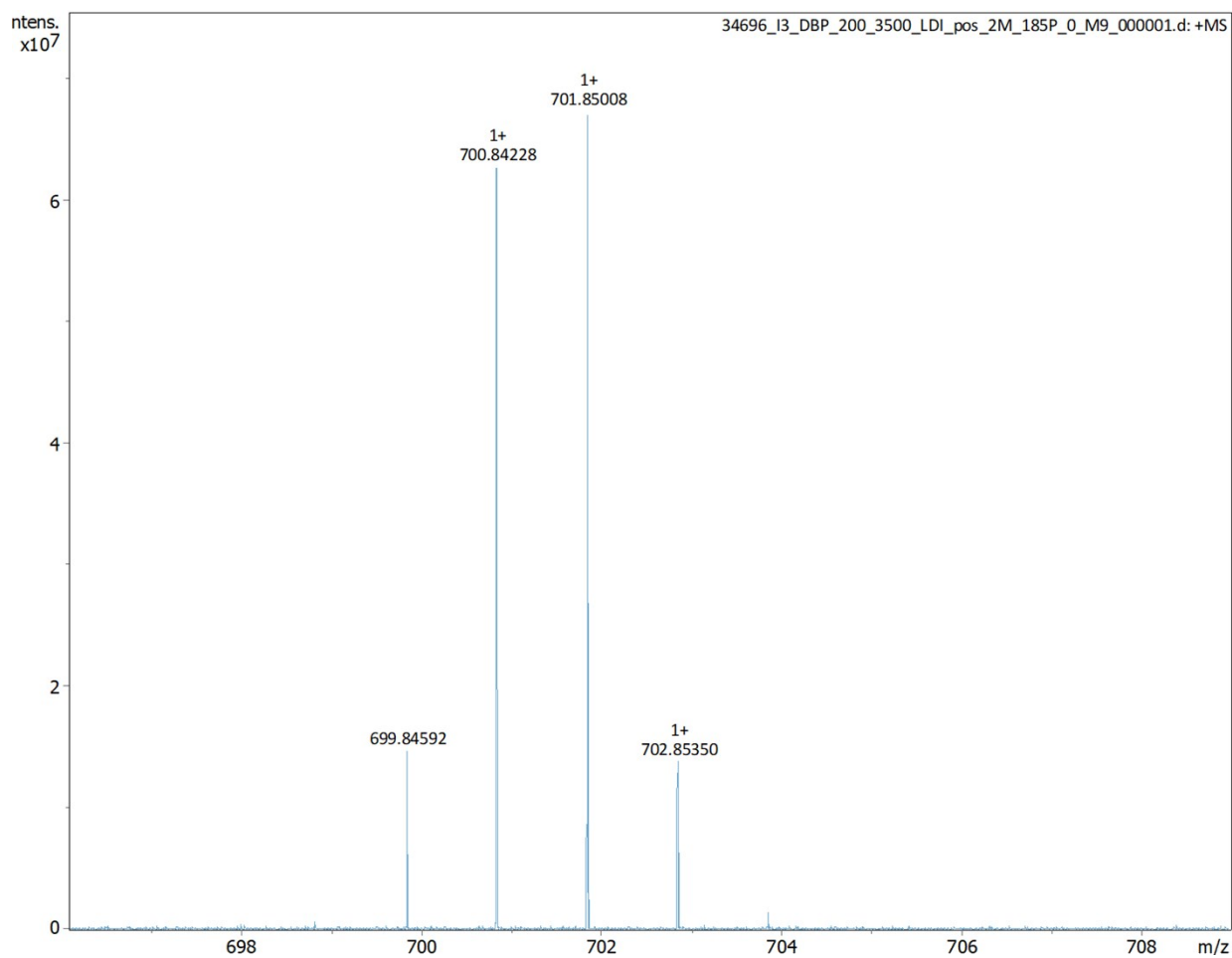
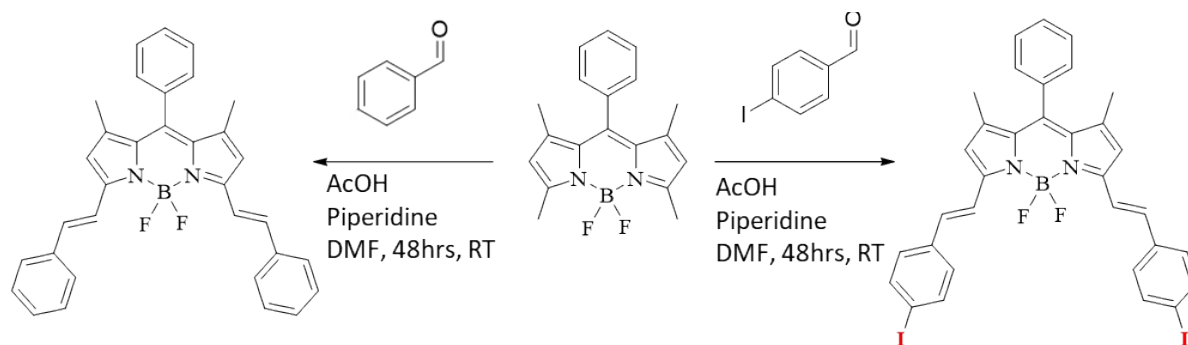


Figure S8. LDI-ToF of $\text{I}_3\text{-BDP}$.



Synthesis of **BDP-0** and **BDP-2**

BDP (150 mg, 0.463 mmol) was dissolved in 10 mL of DMF with either benzaldehyde (196 mg, 1.9 mmol, ~0.2 mL) or 4-iodobenzaldehyde (429 mg, 1.9 mmol) in 20 mL vials for then synthesis of **BDP-0** and **BDP-2**, respectively. Piperidine (0.8 mL) followed by acetic acid (0.8 mL) were added to each solution dropwise via syringe. Reaction was allowed to stir at ambient temperature for 48 hours. Both reactions were extracted with DCM, washed with water and brine. Iodobenzaldehyde based organic layer was washed with saturated aqueous solution of sodium thiosulfate. Organic layers were dried over Na_2SO_4 , dried under vacuum, and purified via silica chromatography with hexanes/ethyl acetate (8:2). Blue eluent with bright red fluorescent solution collected and dried.

BDP-0 yield: 132 mg (57%). ^1H NMR: 7.75 (d, 2H), 7.64 (d, 4H), 7.51-7.50 (m, 3H), 7.41 (t, 4H), 7.33 (d, 4H), 7.26 (d, 2H), 6.65 (s, 2H), 1.45 (s, 6H). MW: 500.4 g/mol. LDI-MS: **BDP-0** calculated mass: 500.22356. Found mass: 500.22370 (0.3 ppm error).

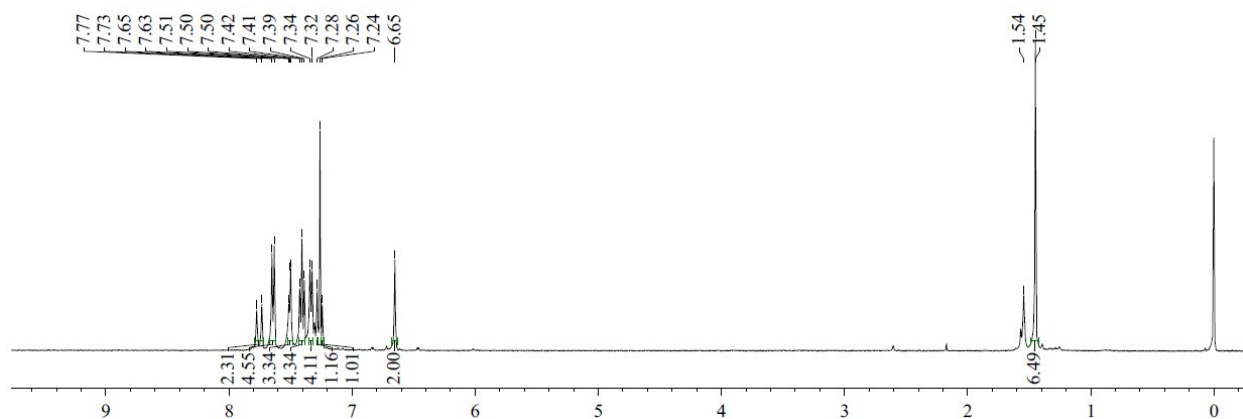


Figure S9. ^1H NMR of **BDP-0**.

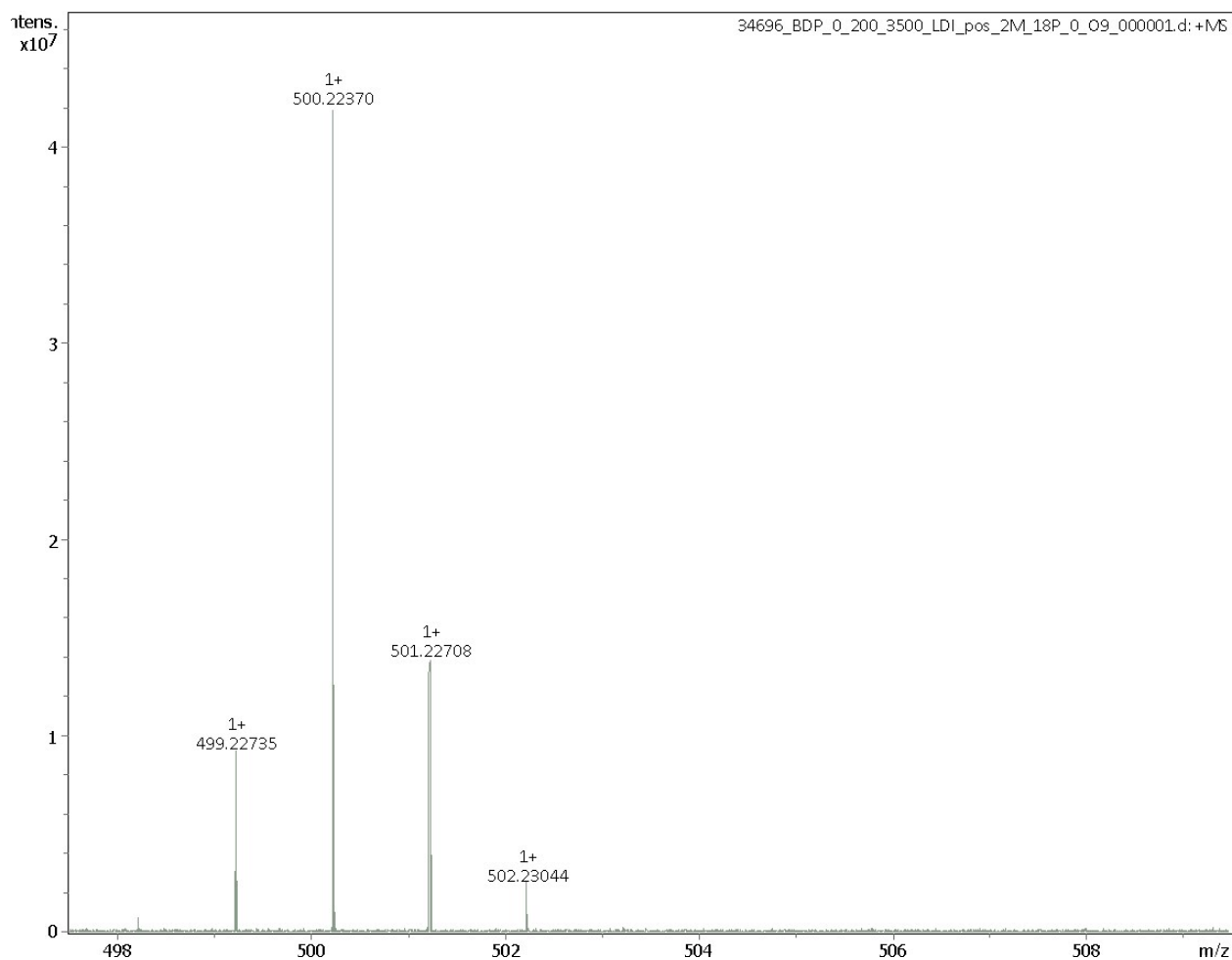


Figure S10. LDI-ToF of **BDP-0**.

BDP-2 yield: 110 mg (32%). ¹H NMR: 7.74-7.70 (m, 6H), 7.51-7.50 (m, 3H), 7.35 (d, 6H), 7.16 (d, 2H), 6.64 (s, 2H), 1.44 (s, 6H). MW: 752.19 g/mol. LDI-MS: **BDP-2** calculated mass: 752.01686. Found mass: 752.01645 (0.5 ppm error).

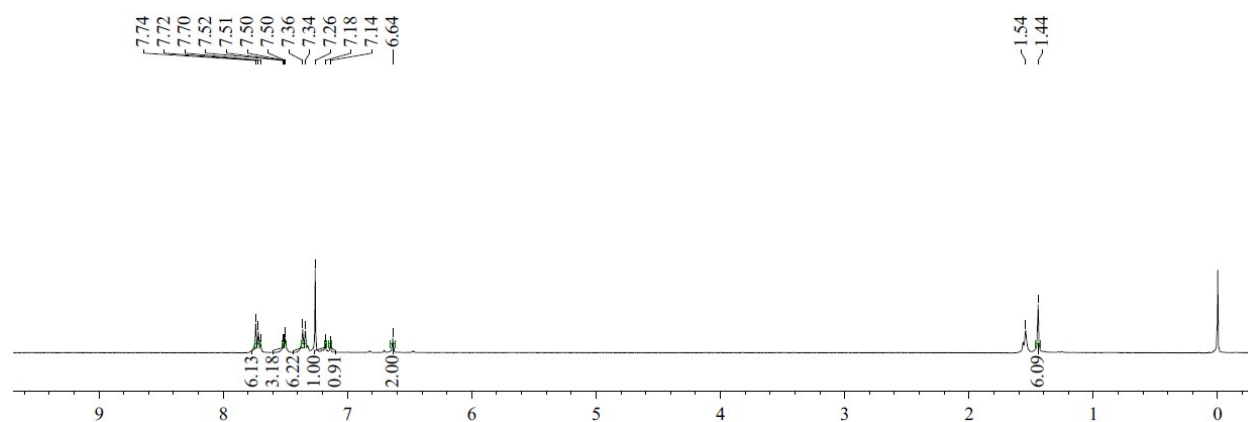


Figure S11. ¹H NMR of **BDP-2**.

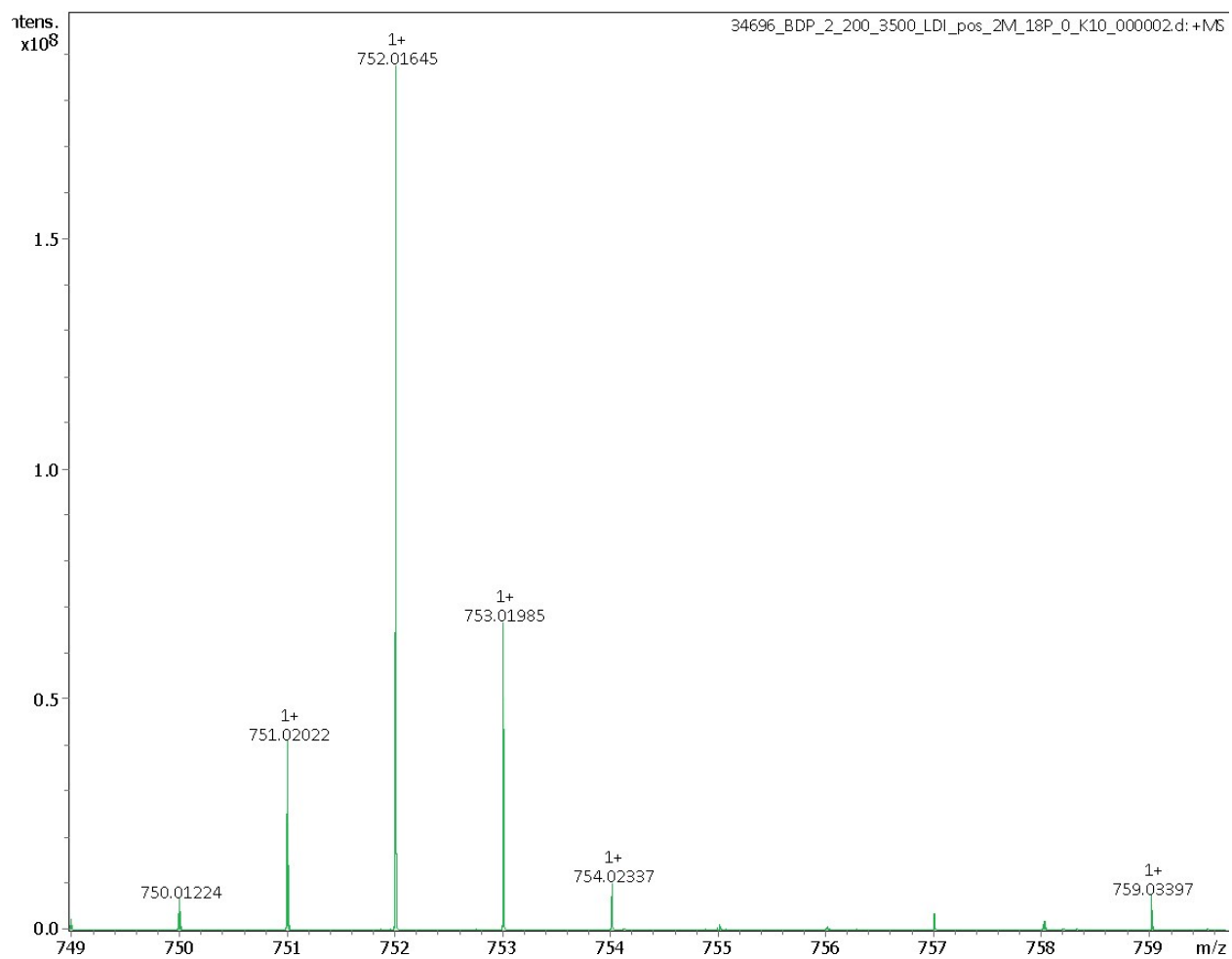
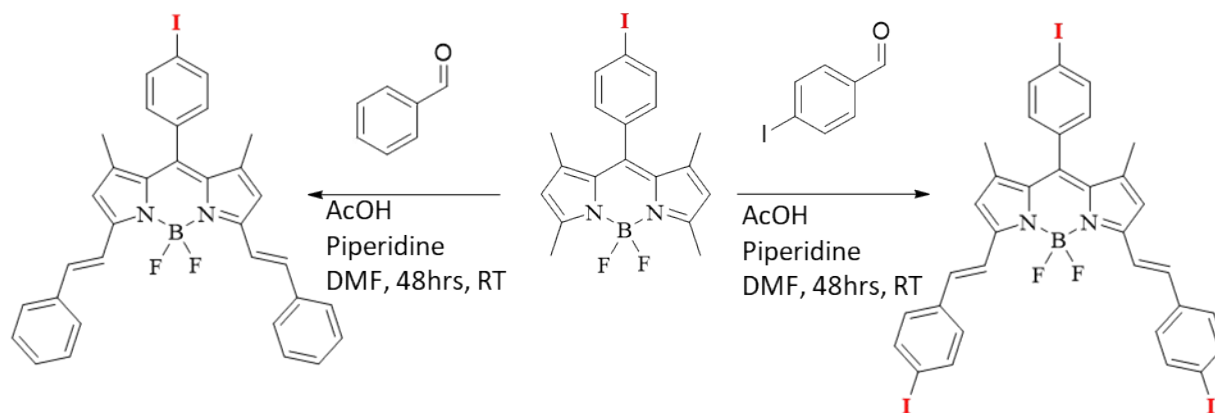


Figure S12. LDI-ToF of BDP-2.



Synthesis of **I-BDP-0** (*unreported*) and **I-BDP-2**

I-BDP (150 mg, 0.33 mmol) was dissolved in 10 mL of DMF with either benzaldehyde (141 mg, 1.33 mmol) or 4-iodobenzaldehyde (309 mg, 1.33 mmol) in 20 mL vials for then synthesis of **I-BDP-0** and **I-BDP-2**, respectively. Piperidine (0.8 mL) followed by acetic acid (0.8 mL) were added to each solution dropwise via syringe. Reaction was allowed to stir at ambient temperature for 48 hours. Both reactions were extracted with DCM, washed with water and brine. Iodobenzaldehyde based organic layer was washed with saturated aqueous solution of sodium thiosulfate. Organic layers were dried over Na₂SO₄, dried under vacuum, and purified via silica chromatography with hexanes/ethyl acetate (7:3). Blue eluent with bright red fluorescent solution collected and dried. **I-BDP-0** yield: 132 mg (63%). ¹H NMR: 7.87 (d, 2H), 7.74 (d, 2H) 7.64 (d, 4H) 7.41 (t, 4H), 7.34 (d, 2H), 7.30 (d, 2H), 7.10 (d, 2H), 6.66 (s, 2H), 1.49 (s, 6H). ¹³C NMR (CDCl₃, 600 MHz): 152.95, 141.90, 138.33, 136.56, 134.71, 133.11, 130.42, 129.03, 128.80, 127.60, 11.21, 118.05, 94.81, 89.97. 89.94, 14.94. MW: 626.30 g/mol. LDI-MS: **I-BDP-0** calculated mass: 626.12021. Found mass: 626.12036 (0.2 ppm error).

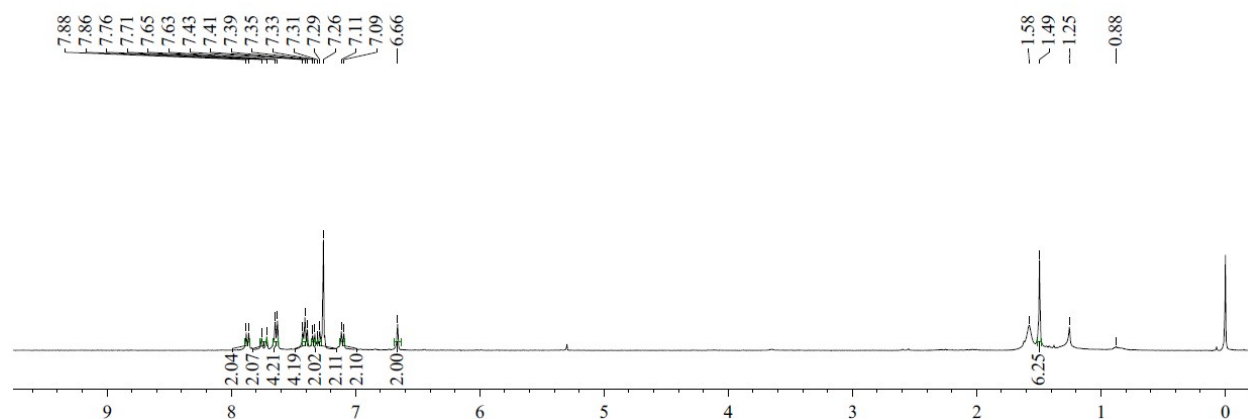


Figure S13. ¹H NMR of **I-BDP-0**.

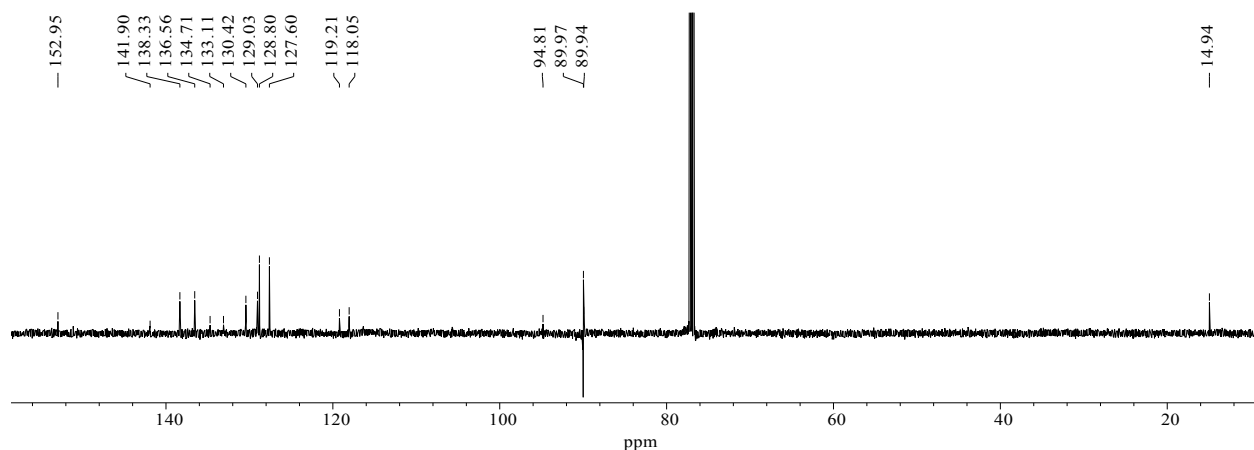


Figure S14. ¹³C NMR of **I-BDP-0**.

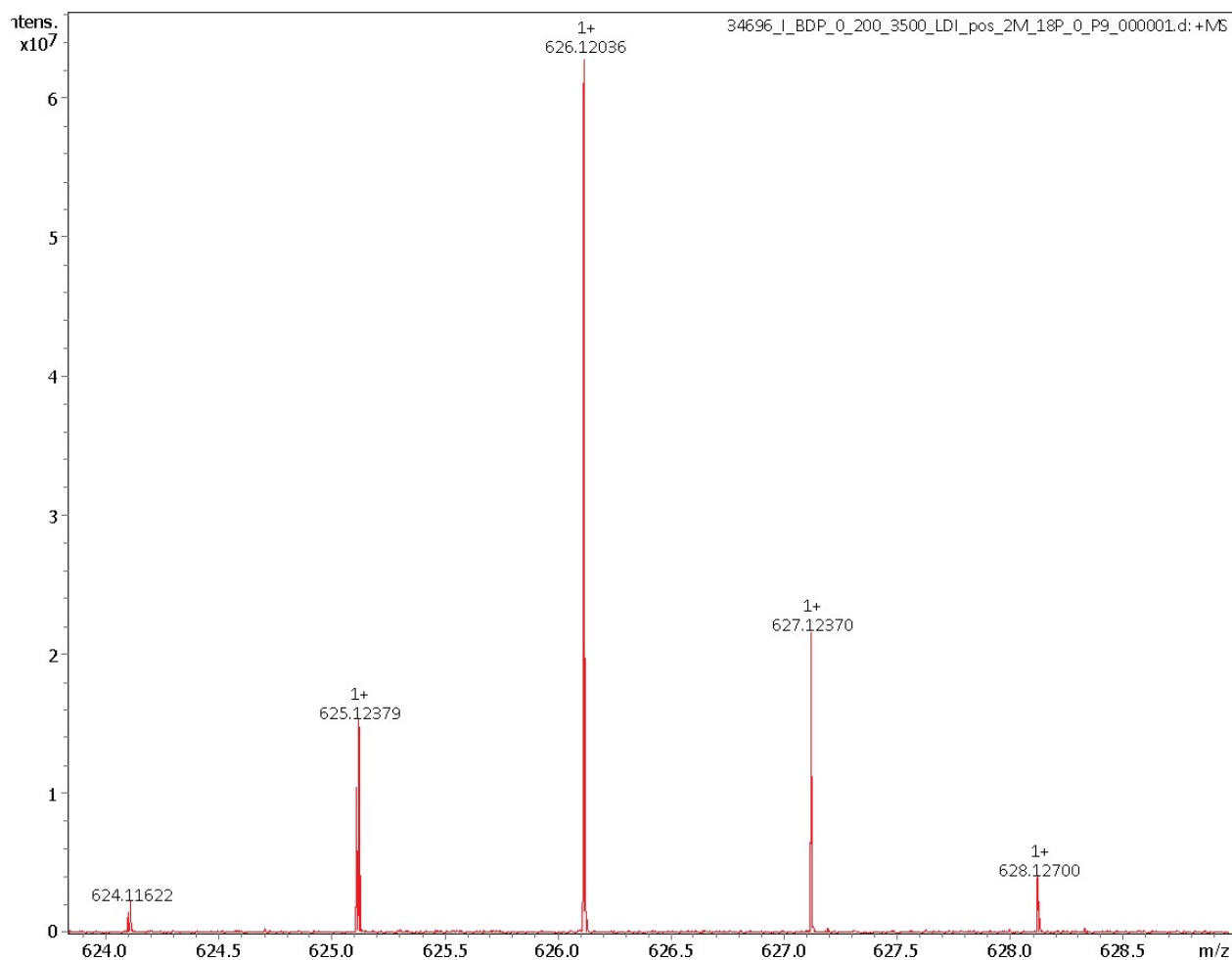


Figure S15. LDI-ToF of I-BDP-0.

I-BDP-2 yield: 140 mg (48%). ¹H NMR: 7.88 (s, 2H), 7.86-7.68 (m, 6H), 7.35 (d, 4H) 7.17 (d, 2H), 7.10 (d, 2H) 6.65 (s, 2H), 1.49 (s, 6H). MW: 878.09 g/mol. LDI-MS: **I-BDP-2** calculated mass: 877.91350. Found mass: 877.91309 (0.5 ppm error).

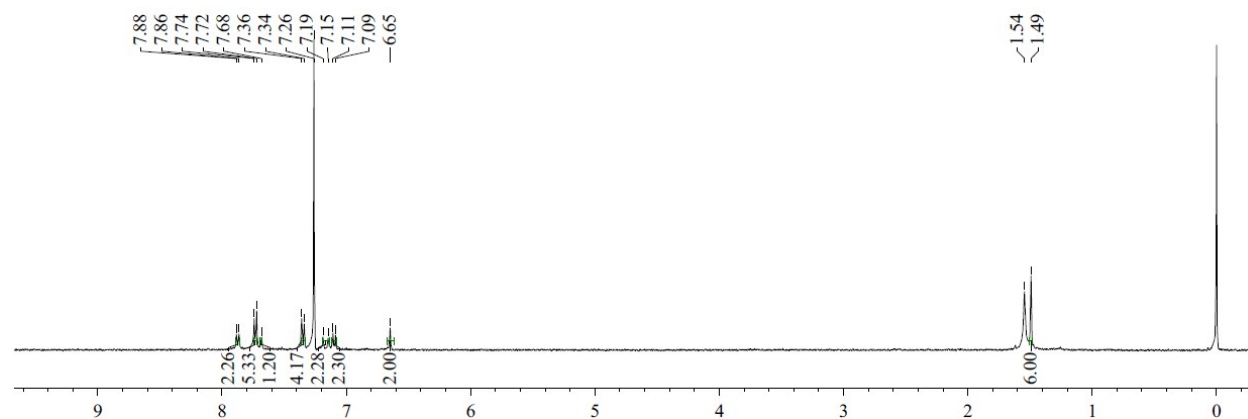


Figure S16. ¹H NMR of I-BDP-2.

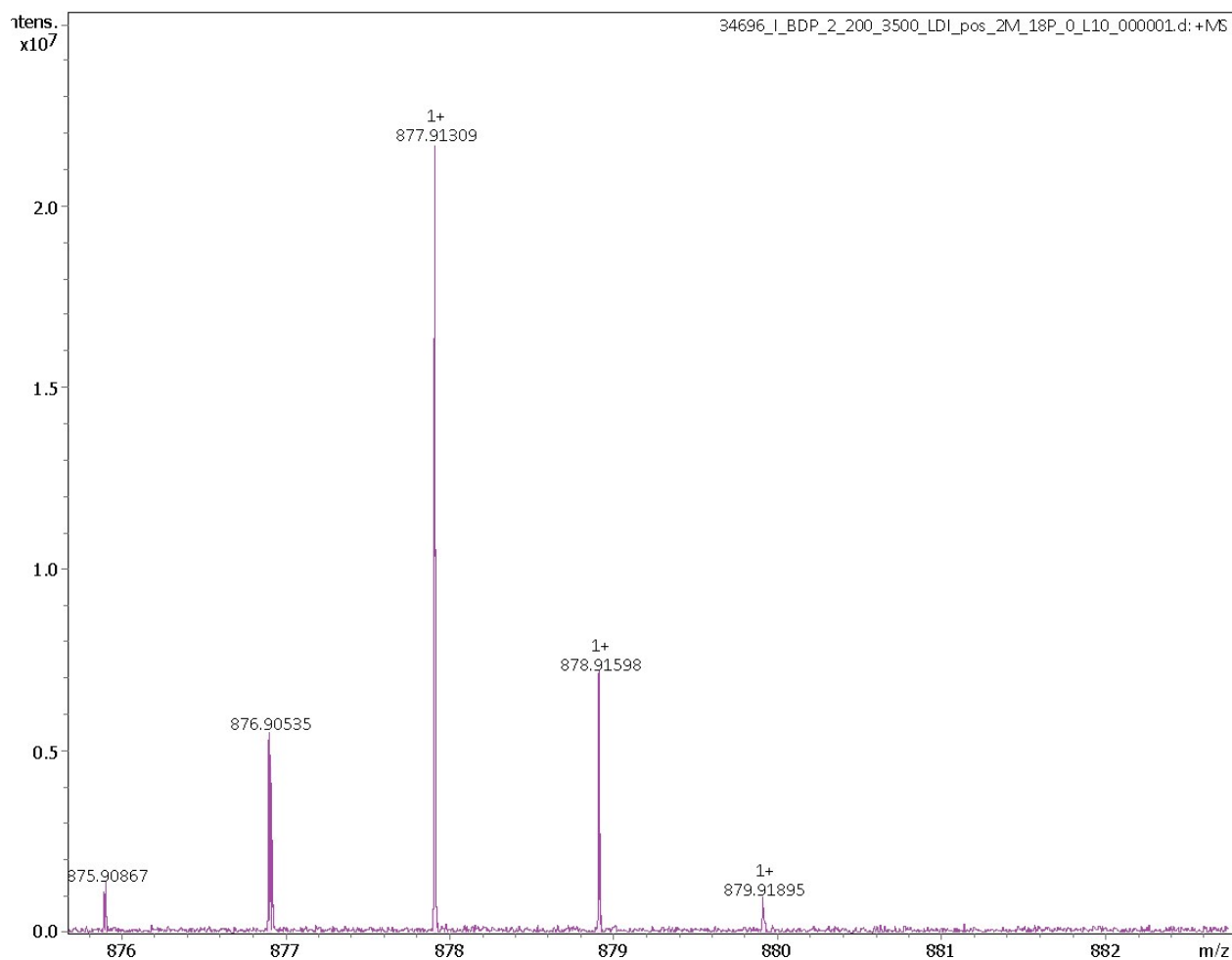
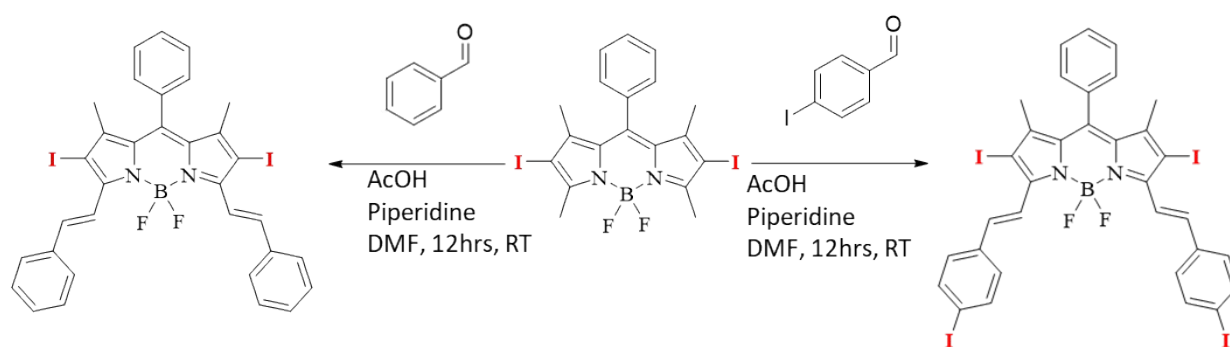


Figure S17. LDI-ToF of I-BDP-2.



Synthesis of I₂-BDP-0 and I₂-BDP-2 (unreported)

I₂-BDP (150 mg, 0.26 mmol) was dissolved in 10 mL of DMF with either benzaldehyde (111 mg, 1.04 mmol) or 4-iodobenzaldehyde (241 mg, 1.04 mmol) in 20 mL vials for then synthesis of I₂-BDP-0 and I₂-BDP-2, respectively. Piperidine (0.8 mL) followed by acetic acid (0.8 mL) were added to each solution dropwise

via syringe. Reaction was allowed to stir at ambient temperature for 12 hours. Both reactions were extracted with DCM, washed with water and brine. Iodobenzaldehyde based organic layer was washed with saturated aqueous solution of sodium thiosulfate. Organic layers were dried over Na_2SO_4 , dried under vacuum, and purified via silica chromatography with hexanes/ethyl acetate (8:2). Blue/green eluent solution collected and dried. **I₂-BDP-0** yield: 106 mg (54%). ^1H NMR: 8.16 (s, 2H), 7.73-7.66 (m, 6H), 7.55-7.54 (m, 3H), 7.43 (t, 4H) 7.37 (d, 2H), 7.32 (d, 2H), 1.46 (s, 6H). MW: 752.22 g/mol. LDI-MS: **I₂-BDP-0** calculated mass: 752.01686. Found mass: 752.01608 (1.0 ppm error).

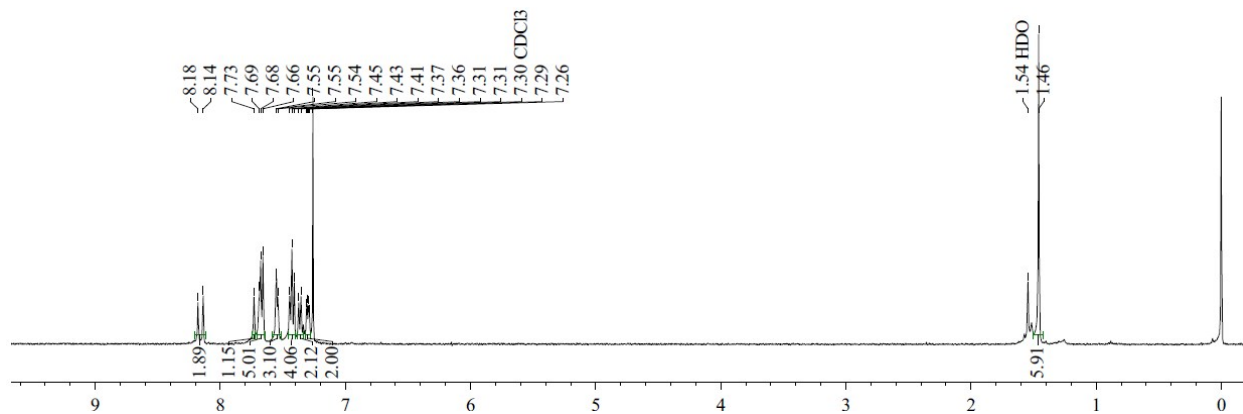


Figure S18. ^1H NMR of **I₂-BDP-0**.

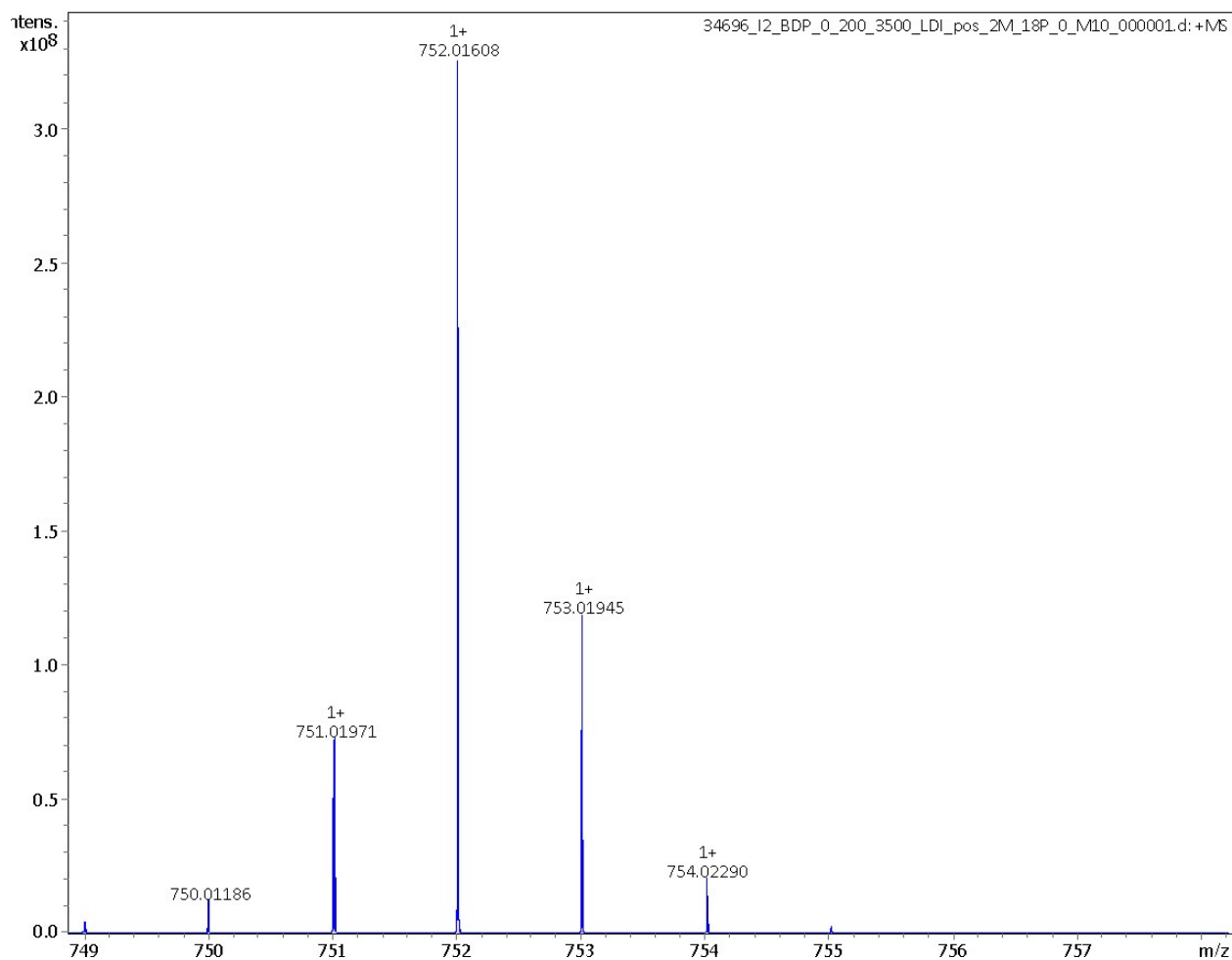


Figure S19. LDI-ToF of **I₂-BDP-0**.

I₂-BDP-2 yield: 95 mg (36%). ¹H NMR: 8.07 (d, 2H), 7.76 (d, 4H), 7.68 (d, 2H), 7.55-7.54 (m, 3H), 7.38 (d, 4H), 7.30-7.28 (m, 2H), 1.45 (s, 6H). Reliable ¹³C NMR was not obtained due to limited solubility in deuterated solvents. MW: 1004.02 g/mol. LDI-MS: **I₂-BDP-2** calculated mass: 1002.80232. Found mass: 1002.80273 (0.4 ppm error).

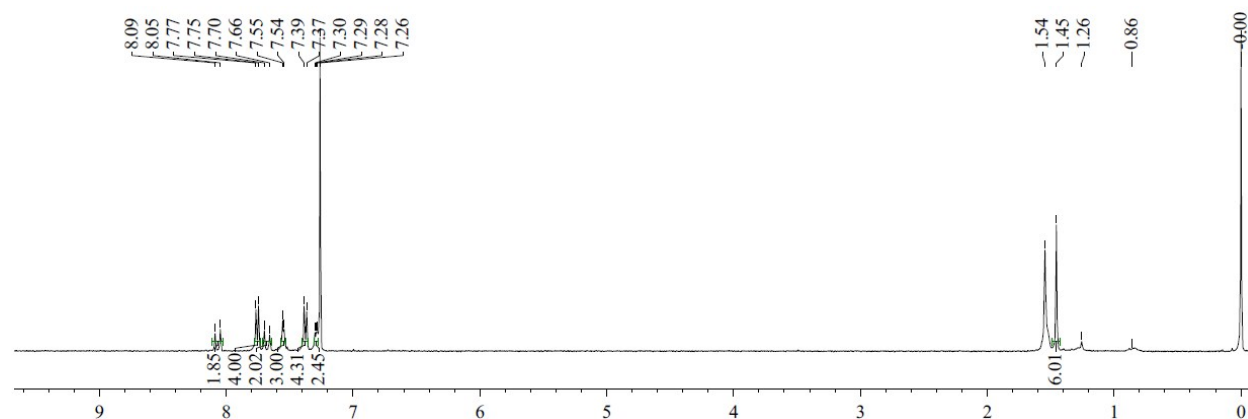


Figure S20. ¹H NMR of **I₂-BDP-2**.

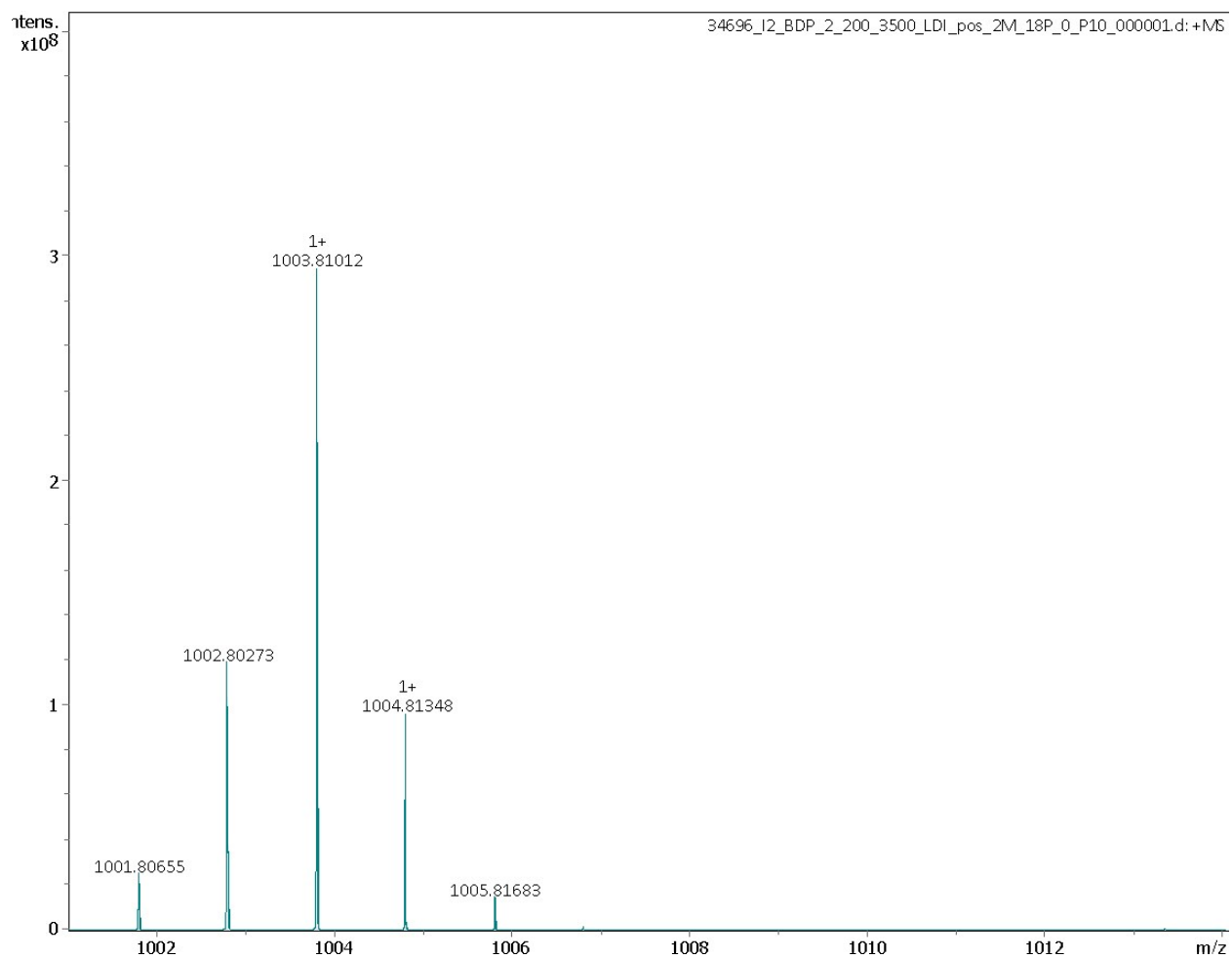


Figure S21. LDI-ToF of I₂-BDP-2.

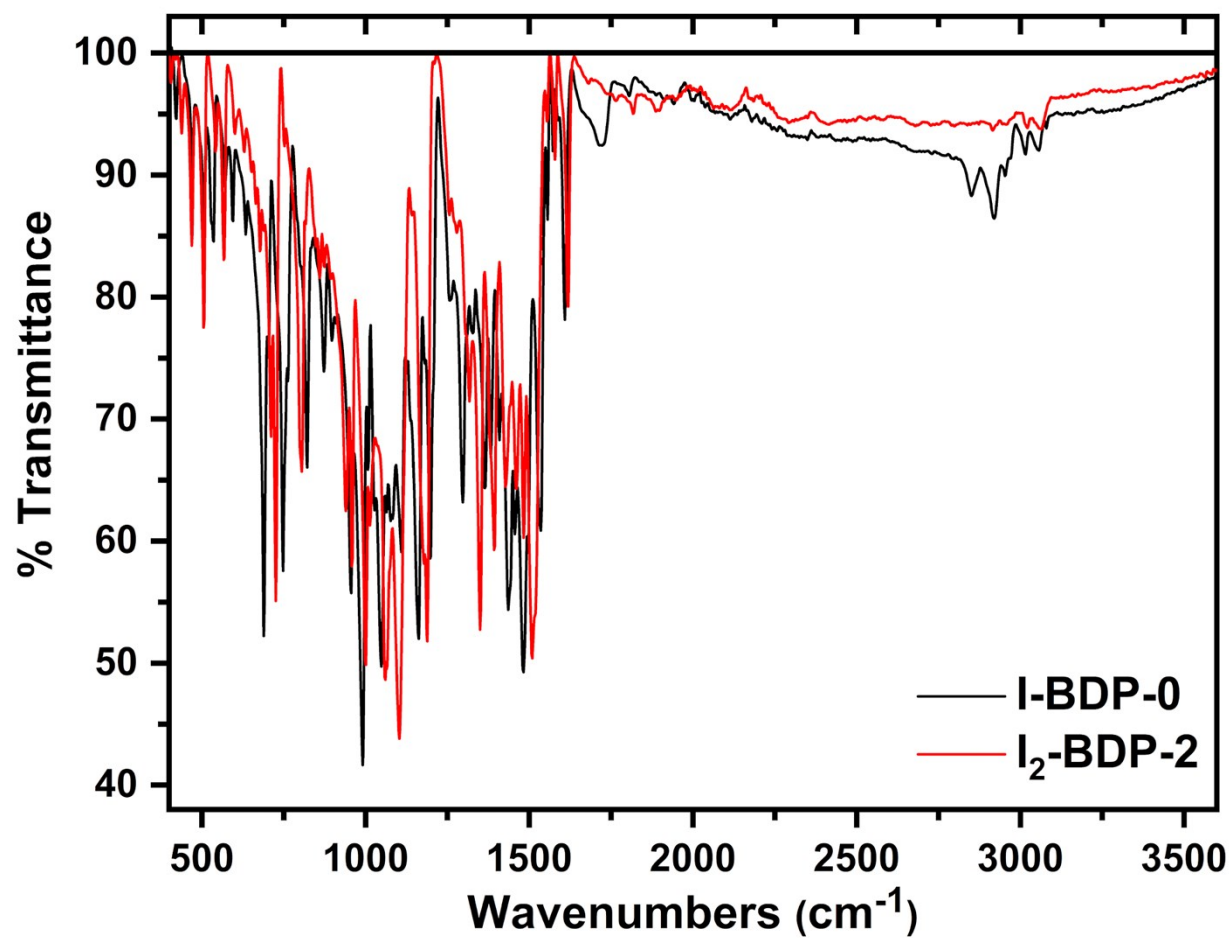


Figure S22. ATR-FTIR spectra of the previously unreported derivatives, I-BDP-0 and I₂-BDP-2.

Supplemental Figures

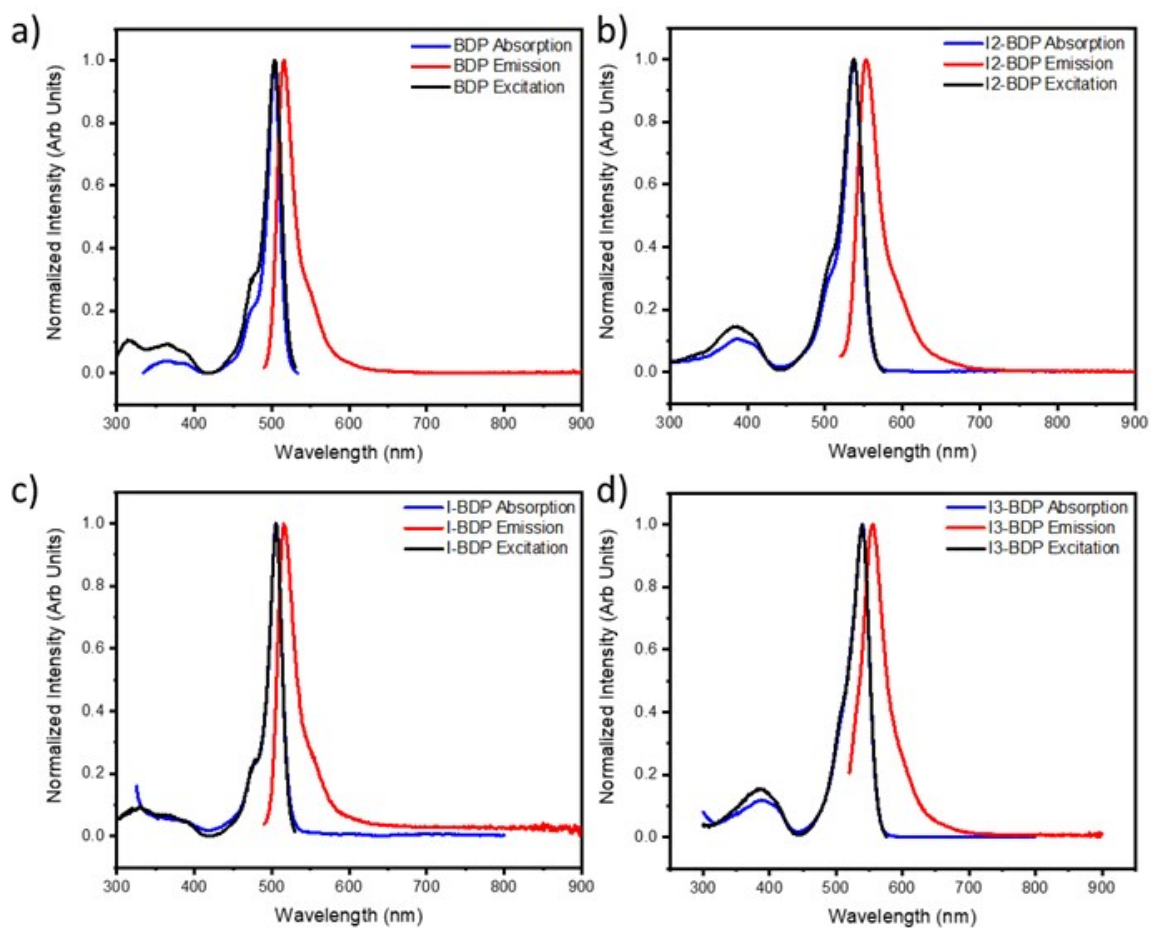


Figure S23. Normalized absorption, emission and excitation spectra of (a) BDP, (b) I₂-BDP, (c) I-BDP, and (d) I₃-BDP.

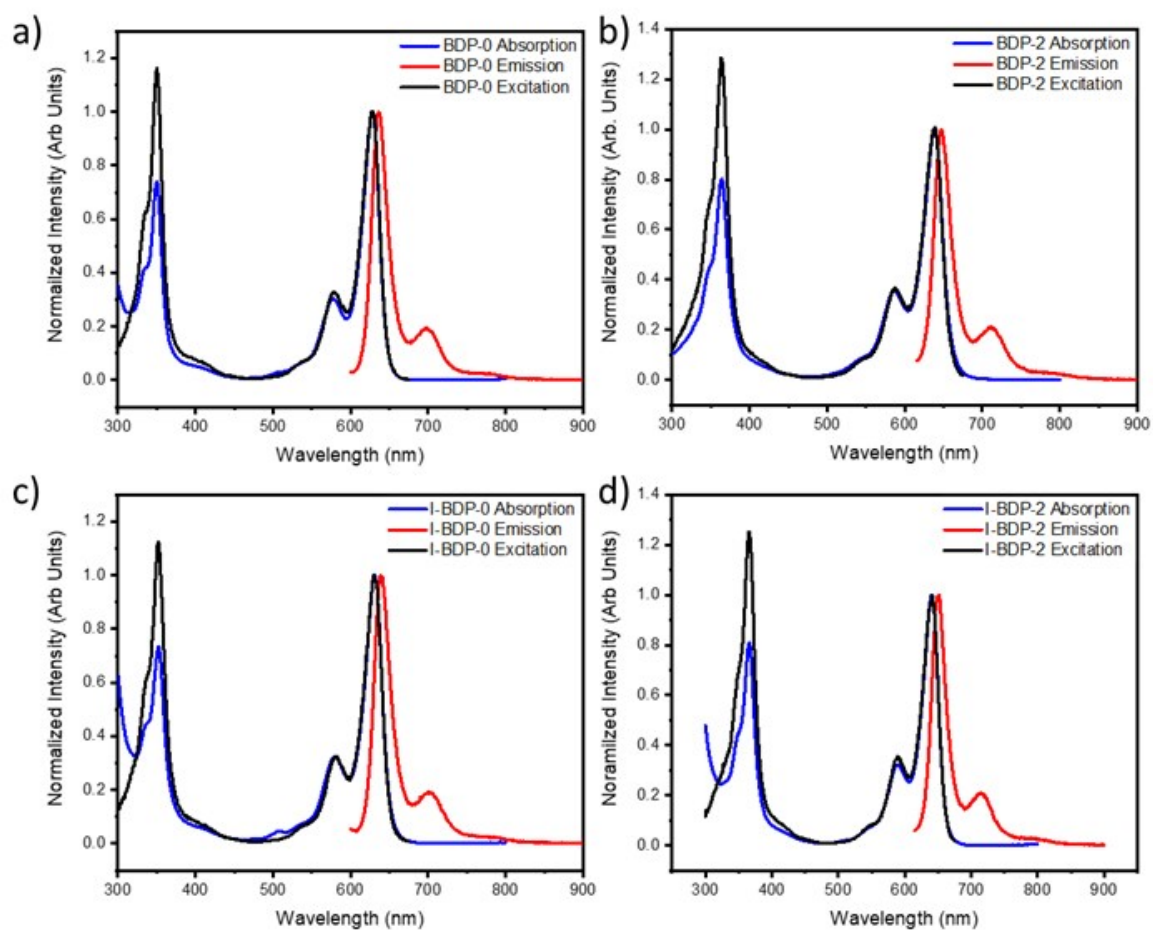


Figure S24. Normalized absorption, emission and excitation spectra of (a) **BDP-0**, (b) **BDP-2**, (c) **I-BDP-0**, and (d) **I-BDP-2**.

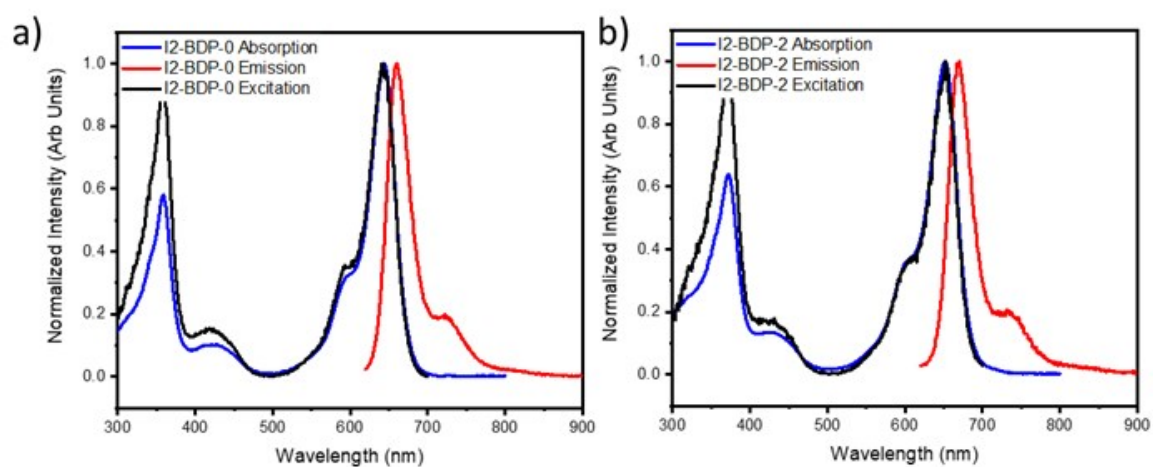


Figure S25. Normalized absorption, emission and excitation spectra of (a) **I₂-BDP-0** and (b) **I₂-BDP-2**.

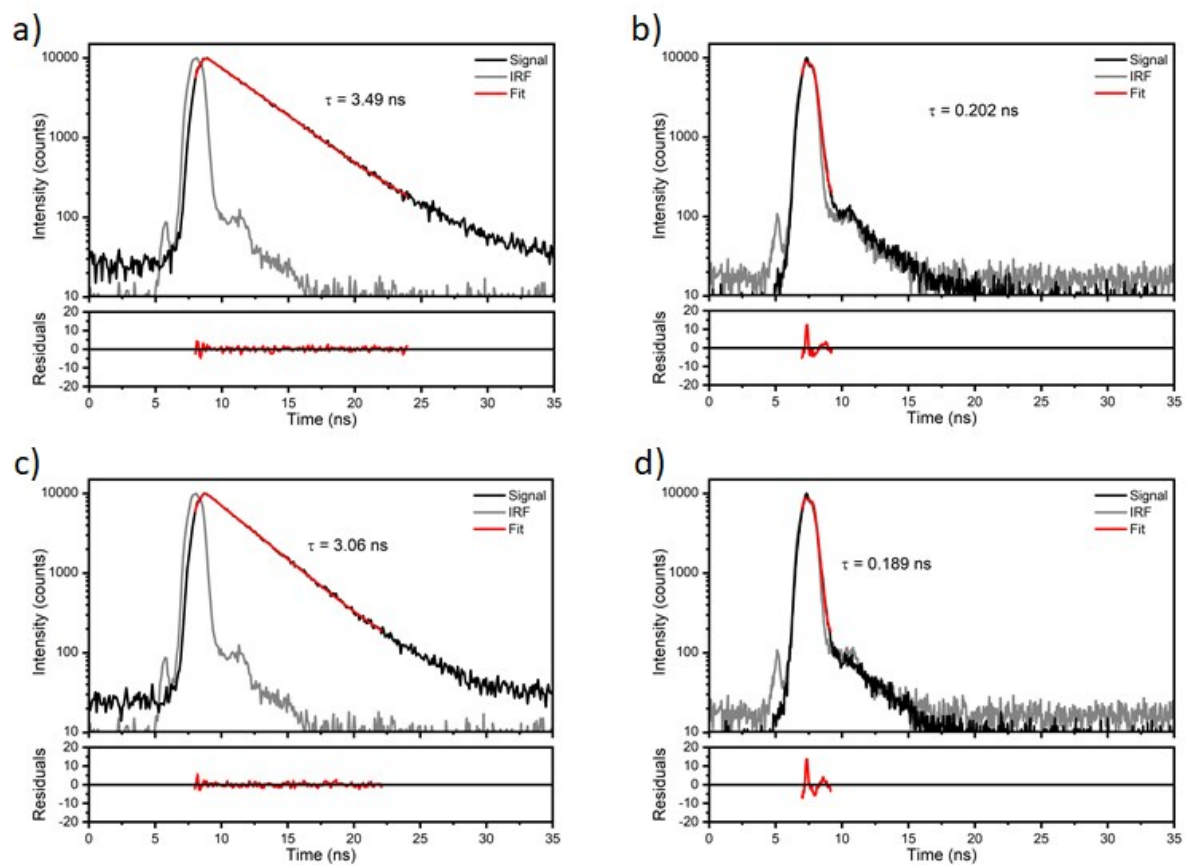


Figure S26. Fluorescence lifetime measurement and fitting residuals of (a) BDP, (b) I₂-BDP, (c) I-BDP, and (d) I₃-BDP via time-correlated single-photon counting.

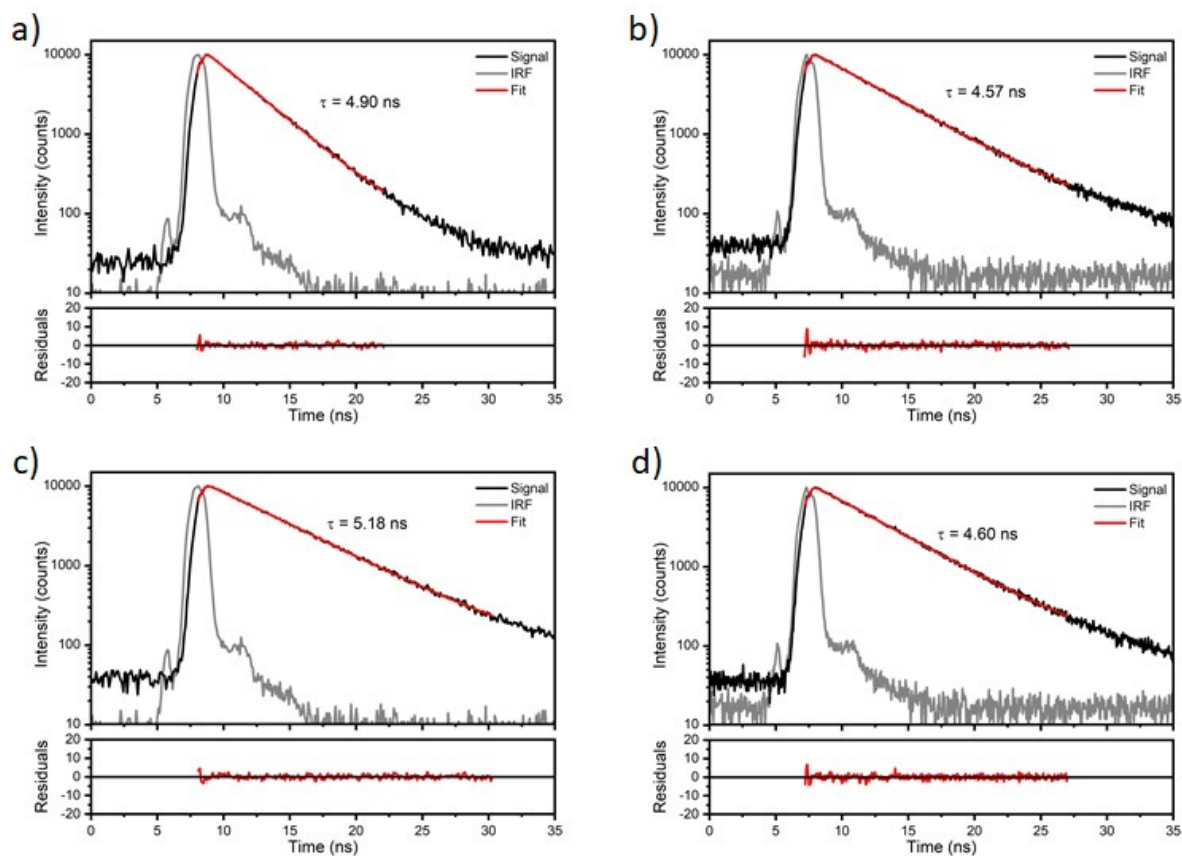


Figure S27. Fluorescence lifetime measurement and fitting residuals of (a) **BDP-0**, (b) **BDP-2**, (c) **I-BDP-0**, and (d) **I-BDP-2** via time-correlated single-photon counting.

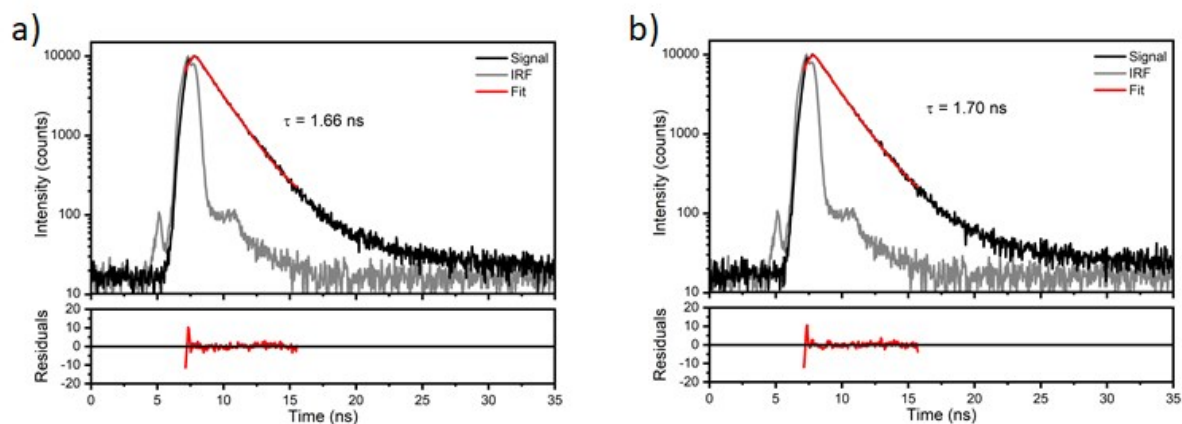


Figure S28. Fluorescence lifetime measurement and fitting residuals of (a) **I₂-BDP-0** and (b) **I₂-BDP-2**

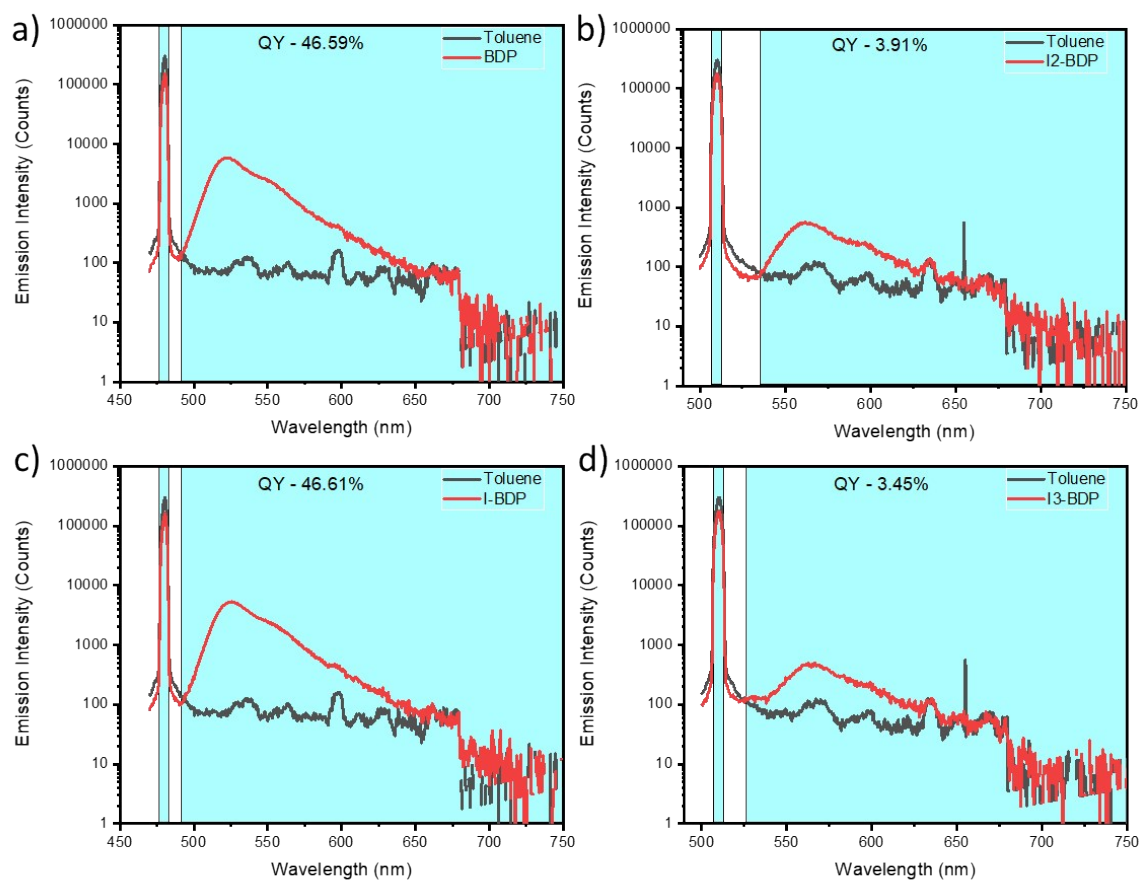


Figure S29. Absolute fluorescence quantum yield of (a) BDP, (b) I₂-BDP, (c) I-BDP, and (d) I₃-BDP with toluene blank as scatter reference.

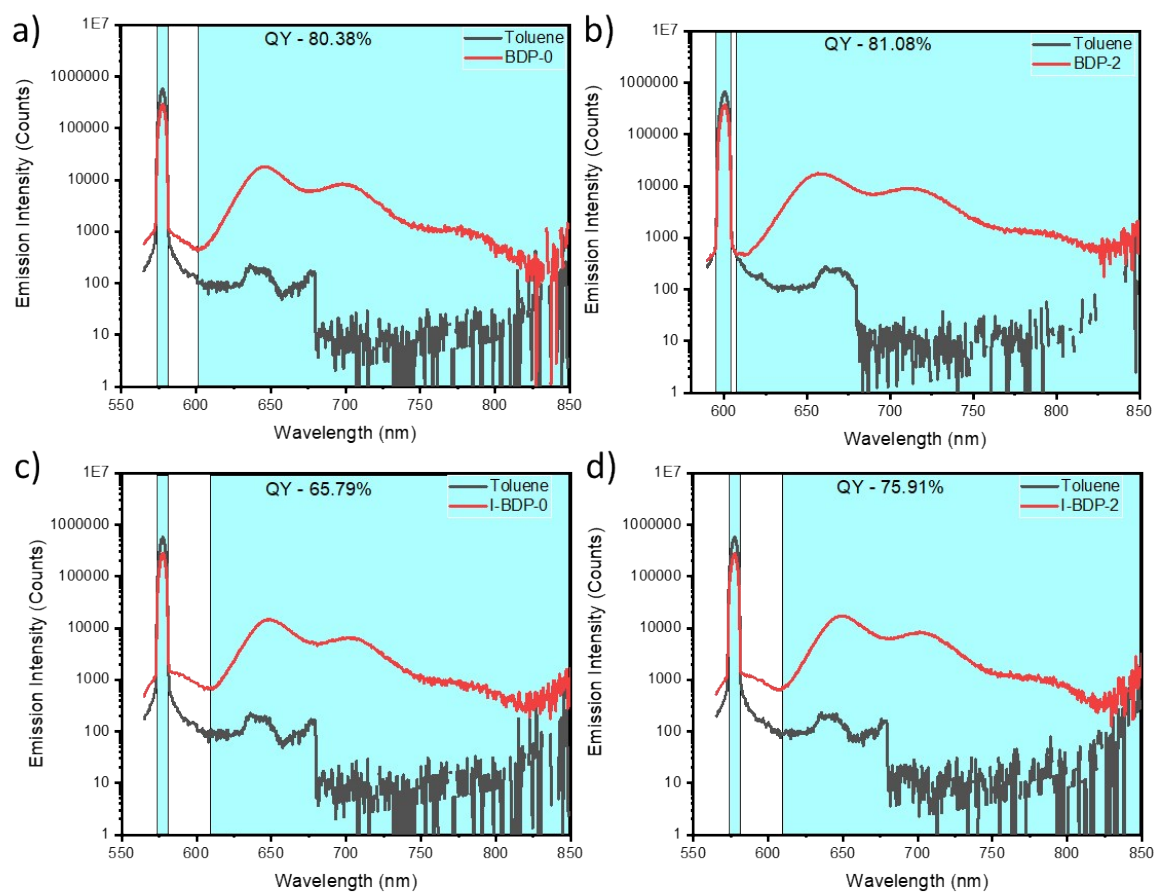


Figure S30. Absolute fluorescence quantum yield of (a) BDP-0, (b) BDP-2, (c) I-BDP-0, and (d) I-BDP-2 with toluene blank as scatter reference.

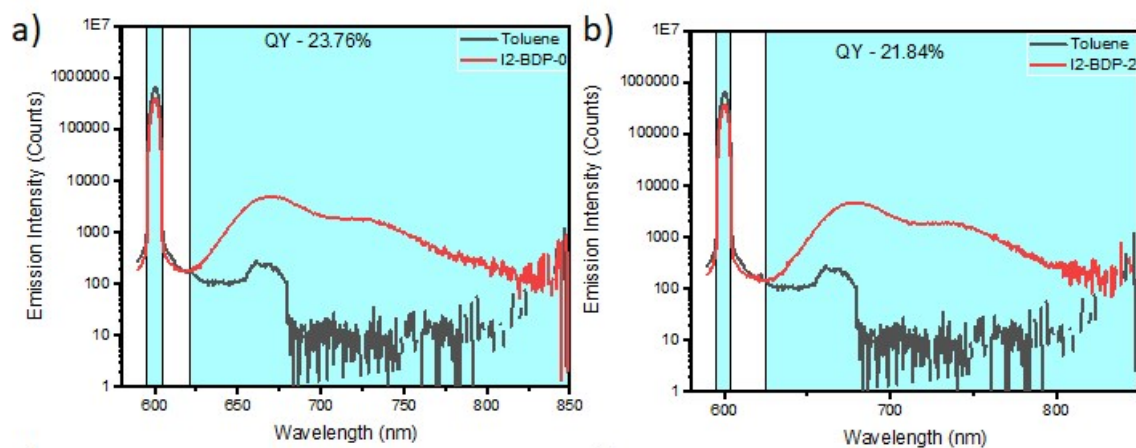


Figure S31. Absolute fluorescence quantum yield of (a) I₂-BDP-0 and (b) I₂-BDP-2.

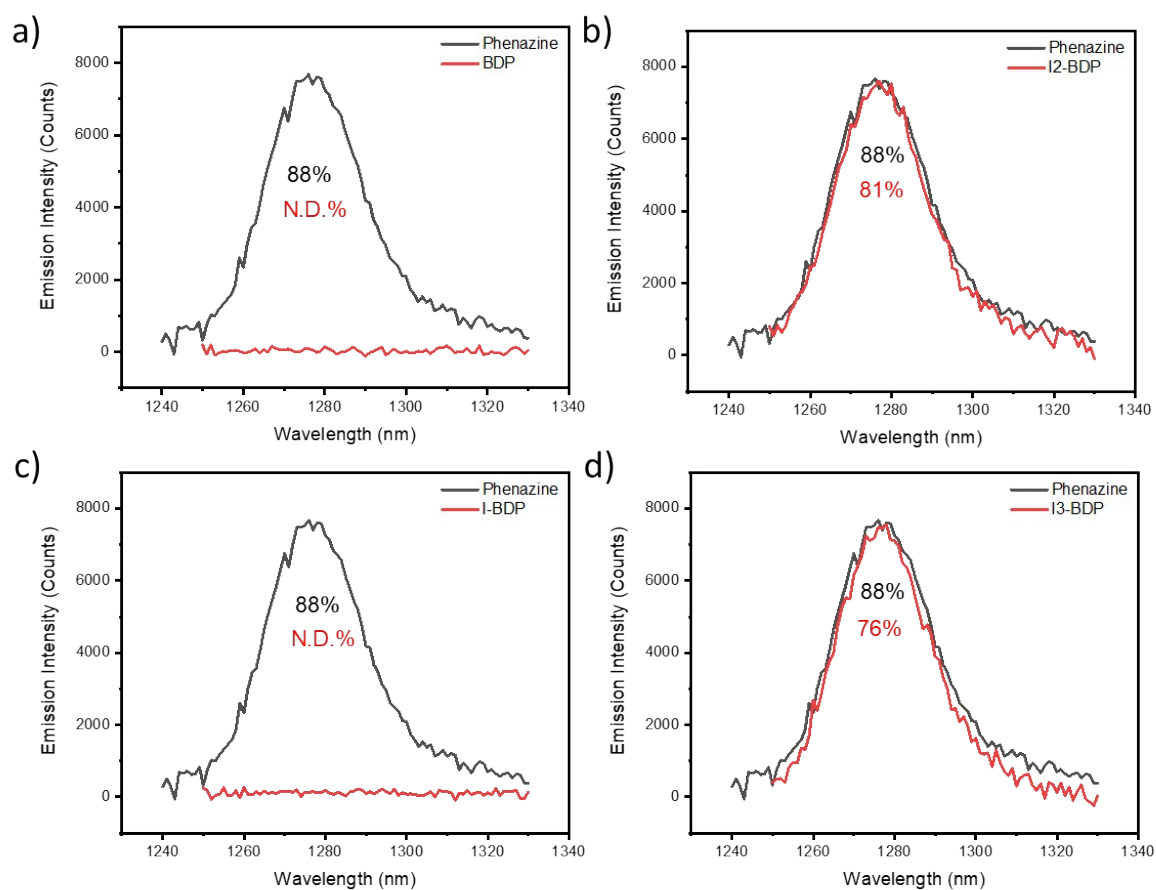


Figure S32. Relative $^1\text{O}_2$ phosphorescence quantum yield of (a) BDP, (b) I₂-BDP, (c) I-BDP, and (d) I₃-BDP with phenazine reference in toluene solution.

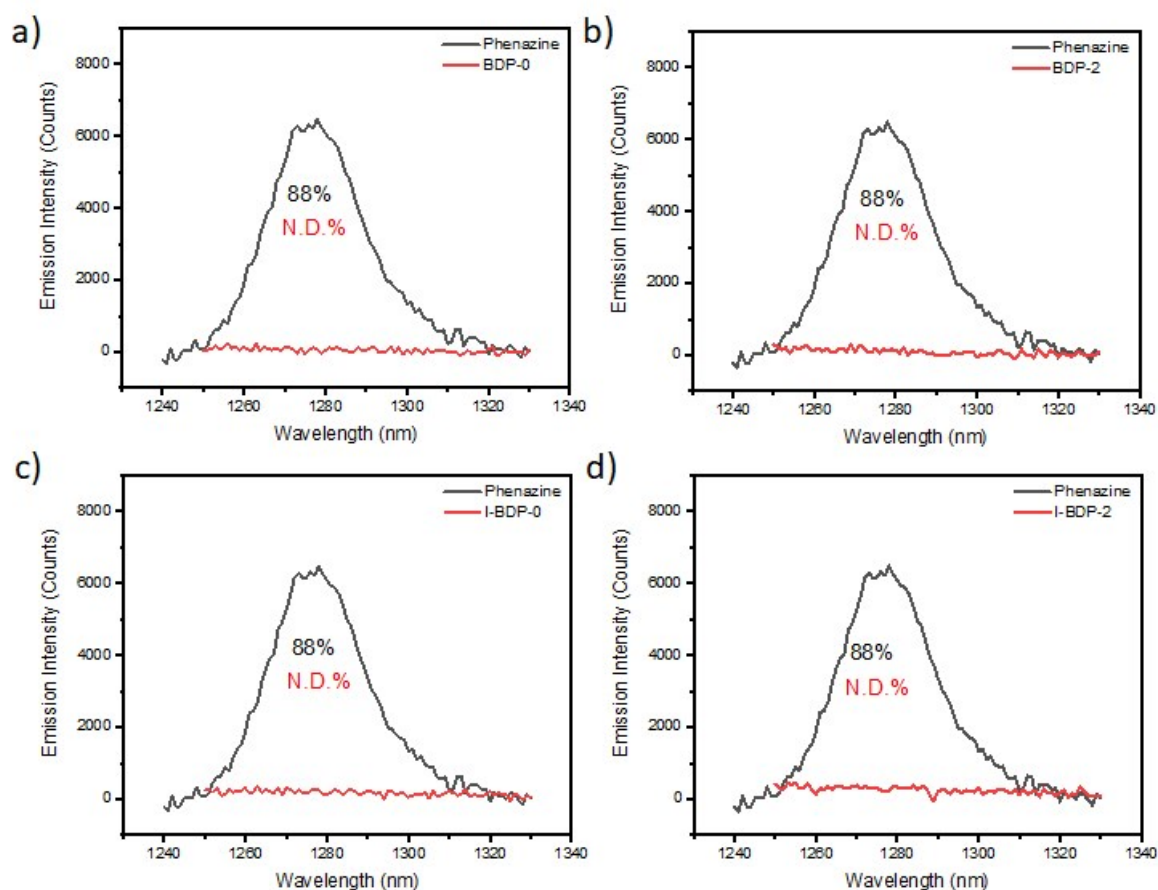


Figure S33. Relative $^1\text{O}_2$ phosphorescence quantum yield of (a) BDP-0, (b) BDP-2, (c) I-BDP-0, and (d) I-BDP-2 with phenazine reference in toluene solution.

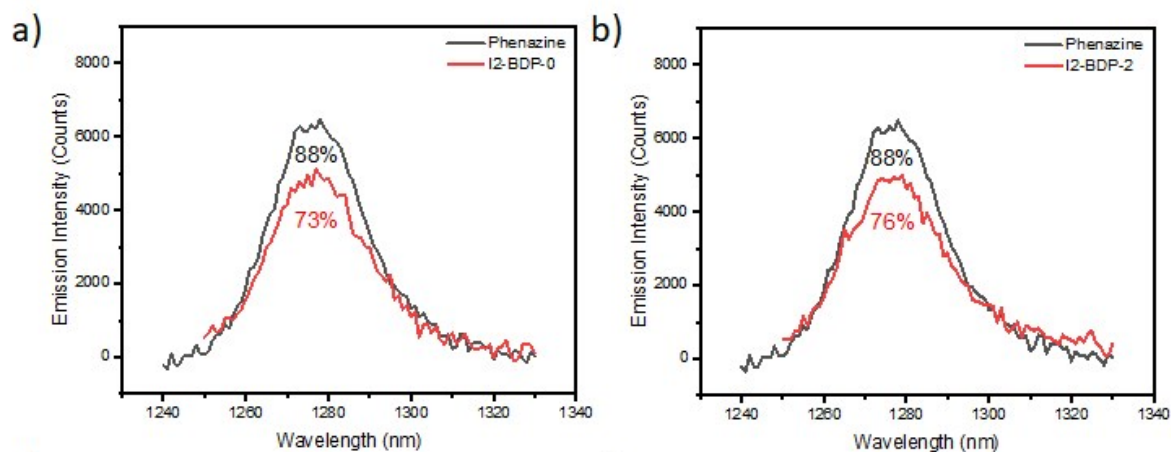


Figure S34. Relative $^1\text{O}_2$ phosphorescence quantum yield of (a) I_2 -BDP-0 and (b) I_2 -BDP-2 with phenazine reference in toluene solution.

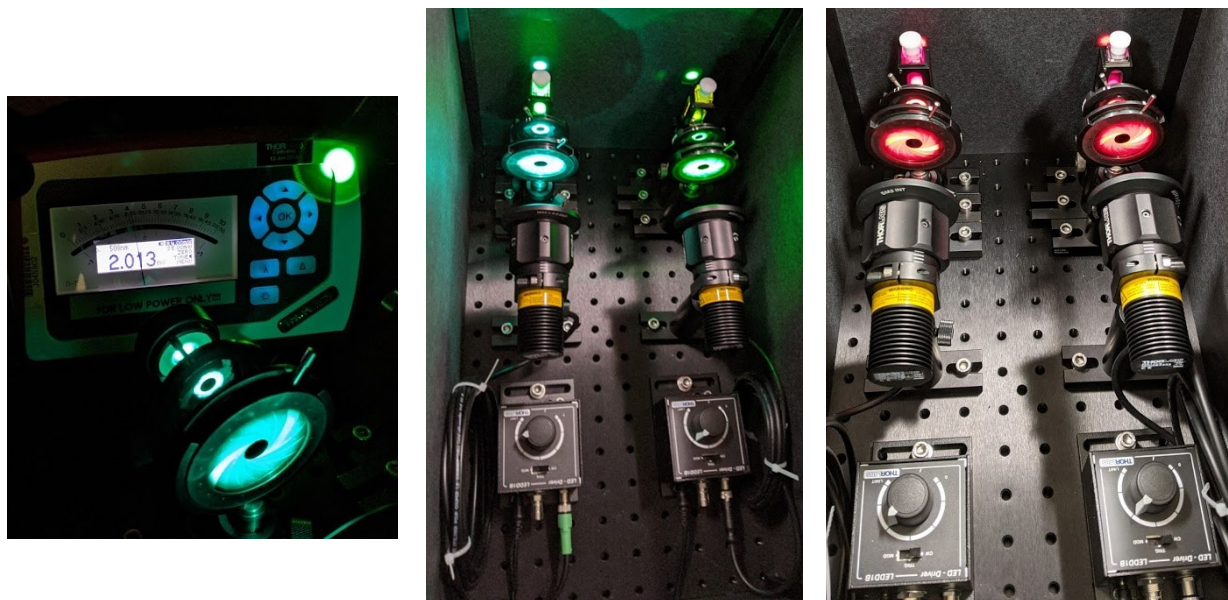


Figure S35. Photos of irradiation set-up with LED power reading (left), photoirradiation of **BDP** and **I₂-BDP** (center), and photoirradiation of red-absorbing **BDP-0** and **I₂-BDP-2** (right).

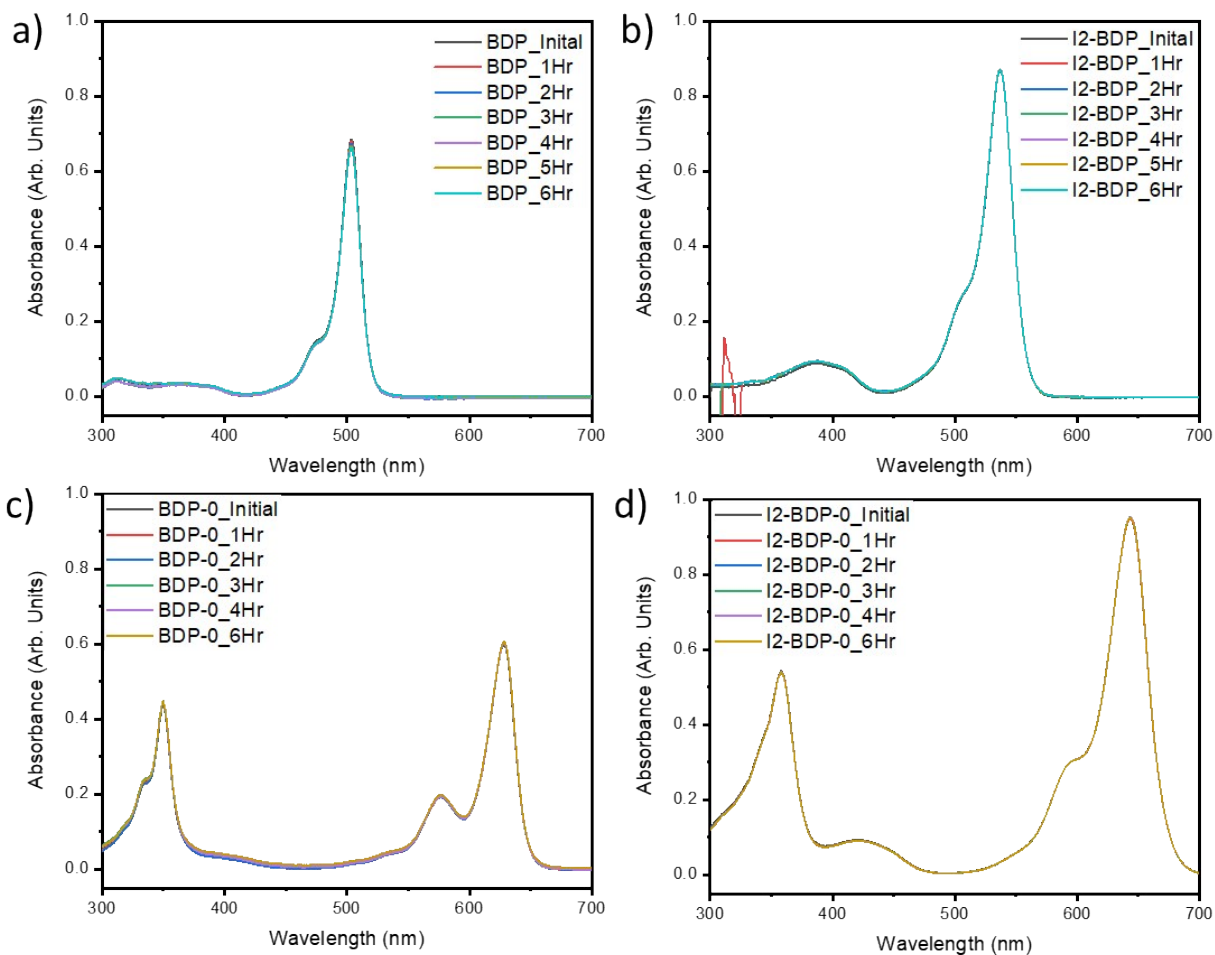


Figure S36. Photodegradation measurement of a) **BDP**, b) **I₂-BDP**, c) **I₂-BDP-0**, and d) **I₂-BDP-2**.

DFT Results

Table S1. BDP molecular orbitals

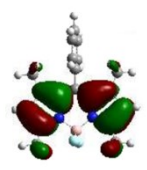
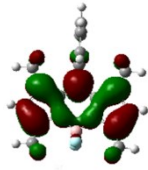
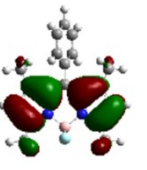
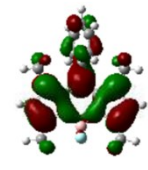
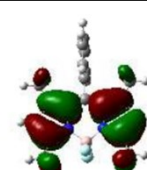
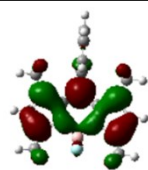
	HOMO	LUMO
Ground State		
S ₁ Optimized State		
	SOMO1	SOMO2
T ₁ Optimized State		

Table S2. I-BDP molecular orbitals

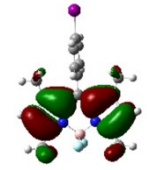
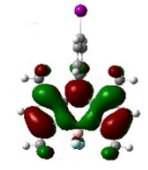
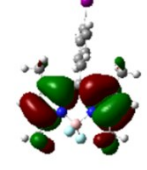
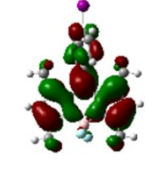
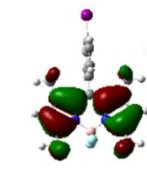
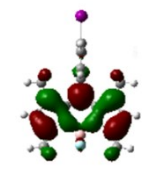
	HOMO	LUMO
Ground State		
S ₁ Optimized State		
	SOMO1	SOMO2
T ₁ Optimized State		

Table S3. I₂-BDP molecular orbitals

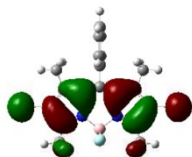
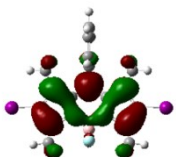
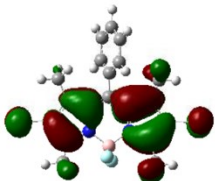
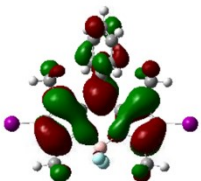
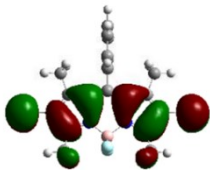
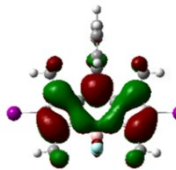
	HOMO	LUMO
Ground State		
S ₁ Optimized State		
	SOMO1	SOMO2
T ₁ Optimized State		

Table S4. I₃-BDP Molecular Orbitals

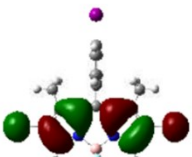
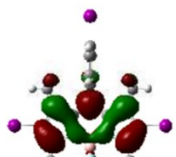
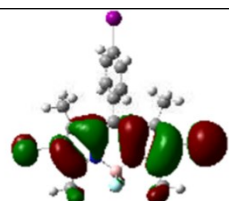
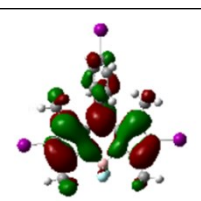
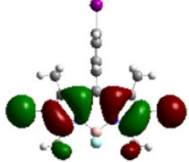
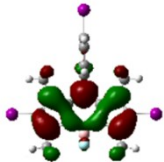
	HOMO	LUMO
Ground State		
S ₁ Optimized State		
	SOMO1	SOMO2
T ₁ Optimized State		

Table S5. BDP-0 molecular orbitals

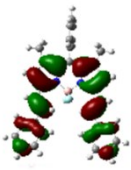
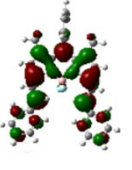
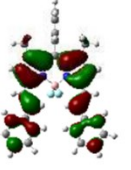
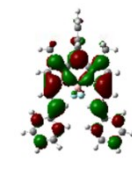
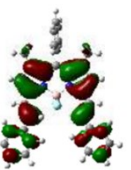

	HOMO	LUMO
Ground State		
S ₁ Optimized State		
	SOMO1	SOMO2
T ₁ Optimized State		

Table S6. I-BDP-0 molecular orbitals

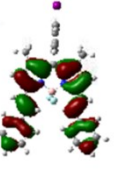
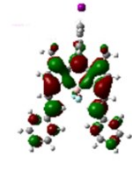
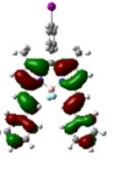
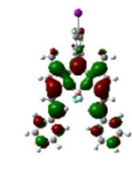
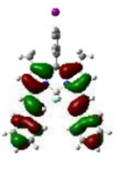
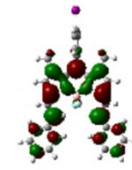
	HOMO	LUMO
Ground State		
S ₁ Optimized State		
	SOMO1	SOMO2
T ₁ Optimized State		

Table S7. BDP-2 molecular orbitals

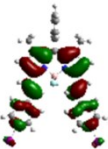
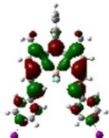
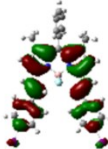
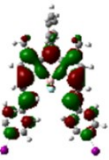
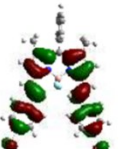
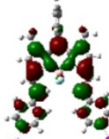
	HOMO	LUMO
Ground State		
S ₁ Optimized State		
	SOMO1	SOMO2
T ₁ Optimized State		

Table S8. I-BDP-2 molecular orbitals

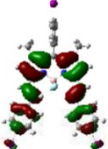
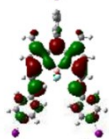

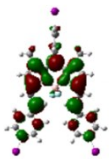
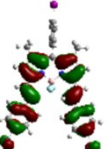
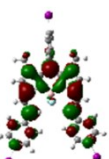
	HOMO	LUMO
Ground State		
S ₁ Optimized State		
	SOMO1	SOMO2
T ₁ Optimized State		

Table S9. I₂-BDP-0 Molecular Orbitals

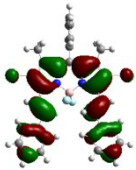
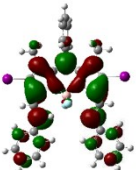
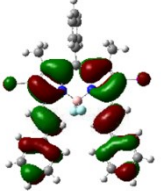
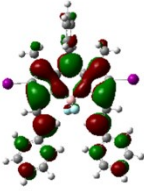
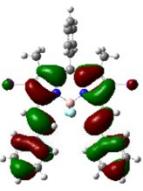
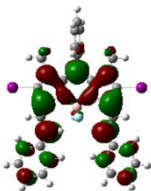
	HOMO	LUMO
Ground State		
S ₁ Optimized State		
	SOMO ₁	SOMO ₂
T ₁ Optimized State		

Table S10. I₂-BDP-2 Molecular Orbitals

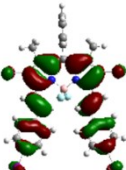
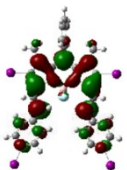
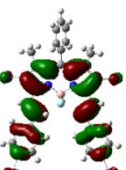

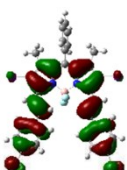
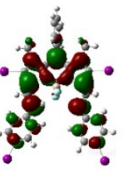
	HOMO	LUMO
Ground State		
S ₁ Optimized State		
	SOMO ₁	SOMO ₂
T ₁ Optimized State		

Table S11. Calculated singlet-state energies, oscillator strengths, triplet-state energies, and singlet-triplet gaps.

		E_{S0-S1} (eV)	Osc str	E_{S0-T1} (eV)	ΔE_{ST} (eV)
Core BDP	BDP	2.82	0.67	1.25	1.57
	I-BDP	2.81	0.67	1.23	1.58
	I ₂ -BDP	2.71	0.84	1.26	1.45
	I ₃ -BDP	2.69	0.84	1.24	1.45
Distyryl-BDP No Triplet	BDP-0	2.17	1.13	0.73	1.44
	I-BDP-0	2.15	1.13	0.70	1.47
	BDP-2	2.15	1.18	0.72	1.43
	I-BDP-2	2.13	1.18	0.70	1.43
Distyryl-BDP Triplet	I ₂ -BDP-0	2.16	1.07	0.82	1.34
	I ₂ -BDP-2	2.14	1.09	0.83	1.31

Table S12. Spin density plots for I₂-BDP and I₂-BDP-0 triplet state.

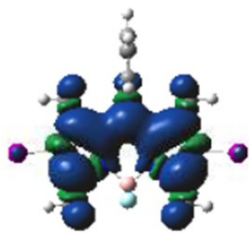
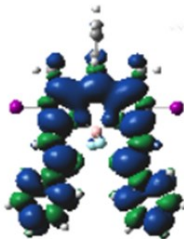
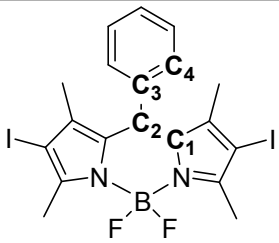
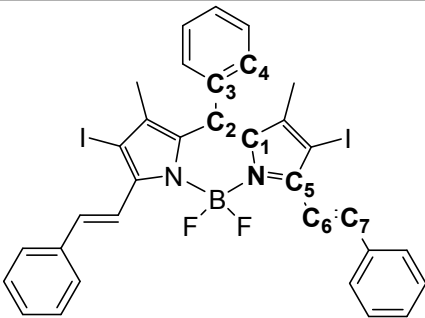
I ₂ -BDP	I ₂ -BDP-0
	

Table S13. Calculated spin density residing on the iodine atom(s) in the triplet-state SOMO₁ orbital.

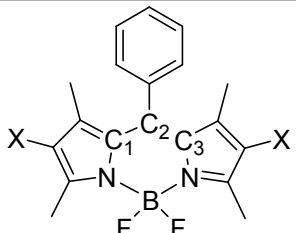
	2,6-position	<i>para</i>-styryl	<i>meso</i>-phenyl	Core spin density	Distyryl spin density
BDP	N/A	N/A	N/A	2.0	N/A
I-BDP	N/A	N/A	2.9×10^{-5}	2.0	N/A
I₂-BDP	0.012	N/A	N/A	2.0	N/A
I₃-BDP	0.013	N/A	3.7×10^{-5}	2.0	N/A
BDP-0	N/A	N/A	N/A	1.28	0.72
I-BDP-0	N/A	N/A	6.9×10^{-5}	1.28	0.72
BDP-2	N/A	0.007	N/A	1.27	0.73
I-BDP-2	N/A	0.007	6.9×10^{-5}	1.27	0.73
I₂-BDP-0	0.007	N/A	N/A	1.26	0.74
I₂-BDP-2	0.007	0.008	N/A	1.25	0.75

Table S14. Calculated ground, optimized S_1 and triplet state geometry data.

						
Compound	$\angle C_1C_2C_3C_4$ ground state ¹	$\angle C_1C_2C_3C_4$ S_1 opt state	$\angle C_1C_2C_3C_4$ T_1 opt state	$\angle NC_5C_6C_7$ ground state	$\angle NC_5C_6C_7$ S_1 opt state	$\angle NC_5C_6C_7$ T_1 opt state
BDP	90	66.0	90	N/A	N/A	N/A
I-BDP	90	62.1	90	N/A	N/A	N/A
I ₂ -BDP	87.1	61.5	90	N/A	N/A	N/A
I ₃ -BDP	87.0	67.5	90	N/A	N/A	N/A
BDP-0	82.9	77.0	82.7	14.6	9.3	8.1
I-BDP-0	82.8	73.9	81.8	14.4	9.2	8.1
BDP-2	82.9	78.0	82.9	14.9	9.5	8.3
I-BDP-2	82.7	73.4	82.0	14.9	9.5	8.4
I ₂ -BDP-0	79.1	73.1	79.8	18.3	10.8	9.5
I ₂ -BDP-2	78.9	74.1	79.9	18.8	11.2	9.7

¹All angles in deg. Highlighted molecules discussed in the main text.

Table S15. Calculated ground, optimized S_1 and triplet state geometry data.

			
Compound	$\angle C_2C_1NB$, Ground State ¹	$\angle C_2C_1NB$, S_1 Opt State	$\angle C_2C_1NB$, T_1 Opt State
BDP	0	7.7	0
I-BDP	0	9.8	0
I ₂ -BDP	1.6 ²	13.7 ³	0
I ₃ -BDP	1.6 ²	8.7 ⁴	0
BDP-0	5.3	7.4	6.7
I-BDP-0	5.3	8.3	6.8
BDP-2	5.4	7.4	6.8
I-BDP-2	5.5	8.2	7.1
I ₂ -BDP-0	2.8	10.2	8.5
I ₂ -BDP-2	6.9	10.1	8.8

¹Angle in deg. Highlighted molecules discussed in the main text.

² $\angle C_2C_3NB = 0.1$ deg

³ $\angle C_2C_3NB = 10.8$ deg

⁴ $\angle C_2C_3NB = 7.5$ deg

References

- 1 S. P. McGlynn, J. Daigre and F. J. Smith, External Heavy-Atom Spin—Orbital Coupling Effect. IV. Intersystem Crossing, *J. Chem. Phys.*, 1963, **39**, 675–679.
- 2 S. P. McGlynn, T. Azumi and M. Kinoshita, *Molecular Spectroscopy of the Triplet State*, Prentice-Hall, Inc., Englewood Cliffs, 1969.
- 3 K. Suzuki, A. Kobayashi, S. Kaneko, K. Takehira, T. Yoshihara, H. Ishida, Y. Shiina, S. Oishi and S. Tobita, Reevaluation of absolute luminescence quantum yields of standard solutions using a spectrometer with an integrating sphere and a back-thinned CCD detector, *Phys. Chem. Chem. Phys.*, 2009, **11**, 9850–9860.
- 4 F. Wilkinson, W. P. Helman and A. B. Ross, Quantum Yields for the Photosensitized Formation of the Lowest Electronically Excited Singlet State of Molecular Oxygen in Solution, *J. Phys. Chem. Ref. Data*, 1993, **22**, 113–262.
- 5 A. M. Brouwer, Standards for photoluminescence quantum yield measurements in solution, *Pure Appl. Chem.*, 2011, **83**, 2213.
- 6 U. Resch-Genger and K. Rurack, Determination of the photoluminescence quantum yield of dilute dye solutions, *Pure Appl. Chem.*, 2013, **85**, 2005–2013.
- 7 Gaussian 16, Revision B.01, M. J. Frisch, G. W. Trucks, H. B. Schlegel, G. E. Scuseria, M. A. Robb, J. R. Cheeseman, G. Scalmani, V. Barone, G. A. Petersson, H. Nakatsuji, X. Li, M. Caricato, A. V. Marenich, J. Bloino, B. G. Janesko, R. Gomperts, B. Mennucci, H. P. Hratchian, J. V. Ortiz, A. F. Izmaylov, J. L. Sonnenberg, D. Williams-Young, F. Ding, F. Lipparini, F. Egidi, J. Goings, B. Peng, A. Petrone, T. Henderson, D. Ranasinghe, V. G. Zakrzewski, J. Gao, N. Rega, G. Zheng, W. Liang, M. Hada, M. Ehara, K. Toyota, R. Fukuda, J. Hasegawa, M. Ishida, T. Nakajima, Y. Honda, O. Kitao, H. Nakai, T. Vreven, K. Throssell, J. A. Montgomery Jr., J. E. Peralta, F. Ogliaro, M. J. Bearpark, J. J. Heyd, E. N. Brothers, K. N. Kudin, V. N. Staroverov, T. A. Keith, R. Kobayashi, J. Normand, K. Raghavachari, A. P. Rendell, J. C. Burant, S. S. Iyengar, J. Tomasi, M. Cossi, J. M. Millam, M. Klene, C. Adamo, R. Cammi, J. W. Ochterski, R. L. Martin, K. Morokuma, O. Farkas, J. B. Foresman and D. J. Fox, Gaussian, Inc., Wallingford CT, 2016.